INFORMATION TO USERS

This manuscript has been reproduced from the microfilm master. UMI films the text directly from the original or copy submitted. Thus, some thesis and dissertation copies are in typewriter face, while others may be from any type of computer printer.

The quality of this reproduction is dependent upon the quality of the copy submitted. Broken or indistinct print, colored or poor quality illustrations and photographs, print bleedthrough, substandard margins, and improper alignment can adversely affect reproduction.

In the unlikely event that the author did not send UMI a complete manuscript and there are missing pages, these will be noted. Also, if unauthorized copyright material had to be removed, a note will indicate the deletion.

Oversize materials (e.g., maps, drawings, charts) are reproduced by sectioning the original, beginning at the upper left-hand corner and continuing from left to right in equal sections with small overlaps.

Finite Element Analysis of a Composite Aerodynamic Bicycle Handlebar

by:

Ling Xie

Department of Mechanical Engineering

McGill University, Montreal

A Thesis Submitted to the Faculty of Graduate Studies and Research in Partial Fulfillment of the Requirements of the Degree of Master of Engineering

Canada

Abstract

An analytical and experimental investigation was conducted to study the design of three different types of aerobars for a composite bicycle.

A Finite Element Analysis software was used for the analysis of the aerobars. Maximum tensile and compression stresses were found in the aerobars that were subjected to three kinds of static load.

A laboratory fabrication method for the aerobar bar-ends was developed, and some sample aerobar bar-ends were made for experimental verification of the analytical results.

The Bicycle Components Test Device was used to perform static tests on the sample aerobar bar-ends under two static load conditions.

Combining the analytical and experimental results, a better understanding of the design and critical problems in the aerobars was obtained.

Resume

Une enquête analytique et expérimentale a été conduite pour étudier la conception de trois types différents d'aerobars pour une bicyclette composée.

Un logiciel fini d'analyse d'élément a été employé pour l'analyse des aerobars. Des efforts maximum de tension et de compression ont été trouvés dans les aerobars qui ont été soumis à trois genres de charge statique.

Une méthode de produit du laboratoire manufacturé des fins d'aerobar de barre a été développée et de l'échantillon aerobar excepté les fins a été fait pour la vérification expérimentale des résultats analytiques.

Le dispositif d'essai de composants de bicyclette a été utilisé pour réaliser les essais statiques sur les barre-extrémités aerobar témoin dans deux conditions de charge statiques.

Combinant les résultats analytiques et expérimentaux, une meilleure compréhension de la conception et des problèmes critiques dans les aerobars ont été obtenus.

Acknowledgements

The accomplishment of this work would not have been possible without the help of several people.

I wish to express my sincere appreciation and gratitude to my thesis supervisor Professor Larry B. Lessard for his precious help, guidance and patience. Special thanks to Professor James Nemes for his availability.

Also special thanks to Steve Kecani for his generous and rapid help in machine work. I am also grateful to the technicians Danen Chellan, Roy Westgate and Tony Micozzi for their instantaneous help in machining.

I wish to thank Marc-Andre Octeau for his continuous help in experimental work. I also wish to thank all the present members of the Composites Materials Group for their help.

Sincere thanks to my husband and son for their understanding and support. I wish to thank my parents and brothers who have continually encouraged and supported me in anything I devoted myself to.

Thanks again to everyone.

TABLE OF CONTENTS

LIST OF TABLES

LIST OF FIGURES

Chapter 1: Introduction

1.1 General Introduction

Traditionally, bicycle is a transportation tool. As it developed into a sporting event, people started to pay attention on its aerodynamic properties.

Aerodynamically, riding a bicycle is like flying. The bicycle has to have high strength, be lightweight, and the position of the rider on the bicycle has to be as streamlined as possible.

Nowadays, more and more people put effort on improving the material and the configuration of bicycle. Composite materials have become one of the main materials for racing bicycles due to their outstanding mechanical properties. Various aerodynamic handlebars (aerobar) have been used to reduce the air drag during the race. Consequently, the rider position has also become a research topic due to the use of aerobar.

This project is to study three types of aerodynamic handlebars used on a composite bicycle. The Finite Element Method is used to predict the stress and displacement of the three aerobars under three static loads. Static tests are performed on sample aerobar bar-ends to verify the Finite Element Analysis results.

1.2 Objective of the Project

The primary goal of this project is

- To perform stress analysis on three different types of aerobars of a composite bicycle under three static load cases, determine the critical stress regions, use the Maximum Principle Stress to examine the current design for a given material, and provide the theoretical basis for the design optimization

- Build some sample aerobar bar-ends, test them using handlebar test equipment, compare the test results with analytical results, and verify the reliability of the FEA

- Provide suggestions for further research and design improvement

1.3 The Reason for Using Composite Materials:

The field of composite materials is growing rapidly. Traditionally, applications of composite materials have originated in weight-critical aerospace structures. More recently, these materials have become popular in various other areas. Over the past three decades, composite materials have been used in many commercial products ranging from high-performance aircraft to sports equipment. The decreasing price of carbon fiber and other fibers used in composites is also broadening the application of composite materials.

Use of composite materials in mechanical design has gained popularity because of several advantages that these materials offer compared to metals. One of the primary reasons is their lightweight property. For example, the density for aluminum is 0.098 lb/in^3 (2.7 g/cm^3) [1], while for high-strength Graphite/Epoxy; it is 0.056lb/in^3 (1.5 g/cm^3) [2], almost a half of the density of aluminum. In addition to their weight advantage per unit volume, most composites provide better stiffness and strength properties compared to metals. For example, the ultimate tensile strength for aluminum is 1.3X10^{4}lb/in^2 (88.9 MPa) [1]. But for high-strength Graphite/ Epoxy, the ultimate tensile strength in fiber direction for unidirectional layer is 2.4X10^{5}lb/in^2 (1641 MPa) [1], almost 20 times of that value for aluminum. That is, structural members made out of composite materials may undergo smaller deformations and carry larger static loads than metal parts.

In the field of cycling, weight reduction is always a serious concern, thus more and more effort has been put into new materials. Also, a bicycle has to be strong enough to withstand the rider's body weight and impact loads. For these reasons, composite materials are one of the best choices for making bicycle frames and components.

1.4 The Reason for Using an Aerobar:

Aerobar is a simplified name for "aerodynamic handlebar" of a bicycle. It is a bar used to enhance the performance of a cyclist during racing by allowing him to put his hands in an aerodynamic position, thus to reduce the air drag dramatically. The aerobar is used in triathlons and various other time trial races.

1.4.1 Difference Between Riding a Traditional Bicycle and a Bicycle with an Aerobar

When riding on a traditional bicycle, one has to put the forearm wide on the handlebar as shown in the following picture. This gesture will form a cavity between chest and thigh; as a result, air drag on the rider's body will be substantial. Thus, this hand position is not ideal, aerodynamically speaking.
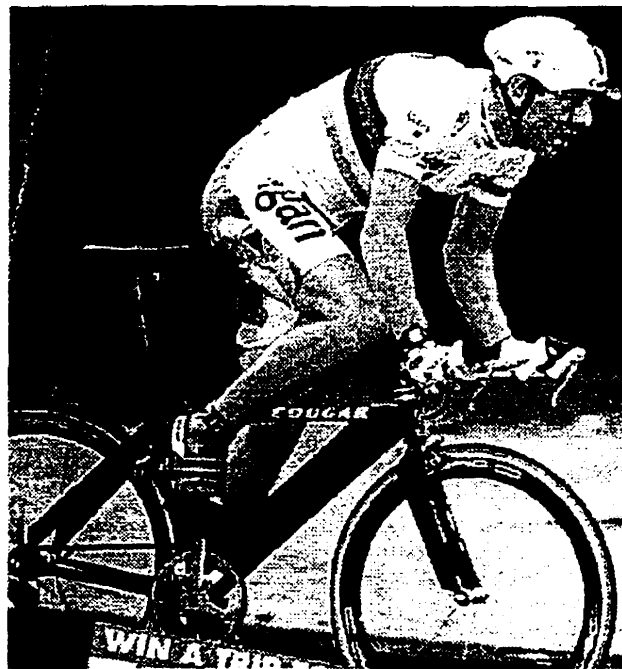
Figure 1.1: Riding on a Traditional Bicycle

While in riding on a bicycle with an aerobar, the rider put the arms together in front of the body and the upper body is much lower than the traditional riding position. In this aerodynamic position, the forearms and the inward elbows make the body more streamlined, as shown in the pictures of Figure 1.2. The frontal area of the body is reduced.
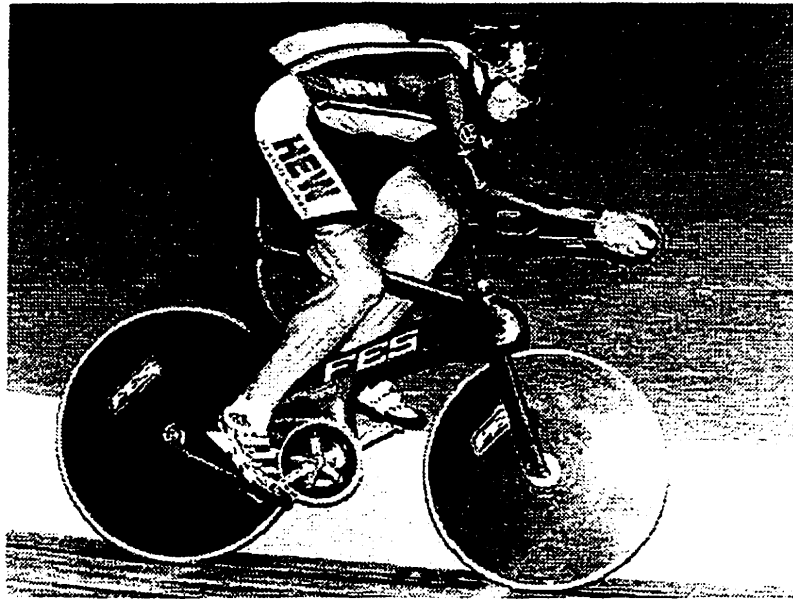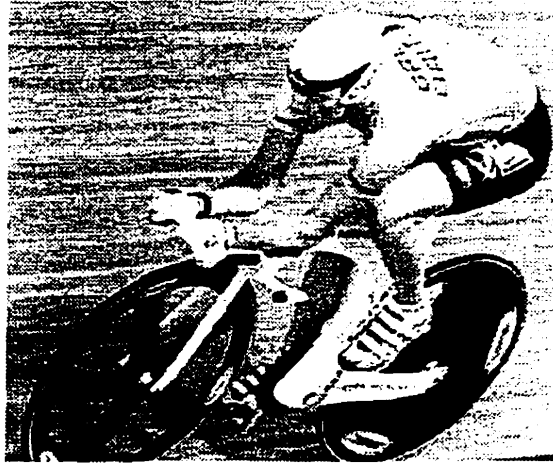
Figure 1.2: Riding On A Bicycle with Aerobar

1.4.2 Benefits From Using an Aerobar

In some sense, riding a bicycle is like flying. As in an airplane, bicycles need to be light, strong and aerodynamic. For this reason, it is not surprising that the first

successful airplane was designed by bicycle mechanics Orville and Wilbur Wright in 1903.

For competitive racing, bicycles need to be as aerodynamic as possible. Research shows that at high speed, wind resistance is the primary impedance factor of motion at ground level. At racing speeds of over 40km/h or higher, wind resistance causes over 90% of the retarding force. Aerodynamic efficiency can minimize air resistance on the front parts of the bicycle, and can reduce energy expenditure and help the rider gain time during the race.

From the knowledge of aerodynamics, in order to be in the best aerodynamic position, one has to keep the back as flat and low as possible without losing power output and comfort. This is called an aero-position. An aerobar is designed for keeping the body in the aero-position. An aerobar utilizes forearm support and is comfortable for maintaining the rider in the aero-position for extended periods of time.

Cyclists benefit from an aerobar and the aero-position because the legs and arms stay relaxed longer when the forearms rather than the upper back and shoulders handle control of the bike. In triathlons, upon finishing the swim, a racer's shoulders and arms may be sore and likely depleted of strength. If the racer rides a bike with aerobar afterwards, he can rest in a position stretched out and balanced on the forearms; therefore not much effort is needed to steer or remain in a straight line [3-8].

1.5 Introduction to Finite Element Method (FEM)

In order to design and analyze aerobars, the Finite Element Method (FEM) will be used extensively.

Due to the complicated geometry of the three aerobars, to predict the stress and deformation everywhere by general methods becomes fairly difficult. FEM is the best method for this project because of its powerful ability for analyzing complex structures.

1.5.1 The necessity of using FEM

Structural designers seek the best design while using the least amount of material. The measurement of success in a design depends on the application. In mechanical design, the design goals are usually related to strength or stiffness. Therefore, the best

design often means the best strength or stiffness for a given application at the lowest cost (i.e., less material used, low material cost, low machining cost, etc.)

Traditionally, engineers evaluated their design according to experience. Nowadays, more scientific and more precise methods are widely used. Engineers can predict the response or status of their design under certain conditions, and furthermore, optimize the design.

In field of mechanics, more and more theories have been established for dealing with the deformation and stress distribution of a particular engineering problem. The final outcome of these theories is basically a set of equations. For a basic problem like beam, shell and plate analysis, the solutions of the equations have been completed based on some reasonable assumptions. Since the actual engineering problems are usually dealing with more complex structures, it is very difficult to derive the appropriate equations to find an exact solution. For these situations, the Finite Element Method was founded, which connects the basic mechanics theory with the complex engineering structures. The creation of the Finite Element Method makes it possible to find an approximate solution for a complicated structural problem.

1.5.2 Introduction to FEM

Finite Element Method is a numerical method, which can be used to find the approximate solution of complex engineering problems. The method was first developed in 1956 for the analysis of aircraft structural problem [9]. Now this method is widely used in various engineering fields, such as civil engineering, mechanical engineering and electrical engineering.

The basic idea in the Finite Element Method is to find the numerical solution of a complicated problem by replacing it by a number of smaller, simpler problems. The solution found is an approximate solution rather than an exact one.

In the Finite Element Method, the whole structure is considered to be building up of many small, interconnected pieces called Finite Elements. Adjacent elements are considered to be connected each other at specified joints, and these joints are called Nodes. Generally, the precision of the solution becomes better as the number of the

6

elements increases. If the number of elements is big enough, the approximate solution will converge to an accurate one.

Usually, the actual variation of the field variable such as displacement and stress of the actual structure are not known, so we replace the actual complicated structure with many Finite Elements and assume that the variation of the field variables inside the Finite Elements can be approximated by a simple function. These approximating functions are defined in terms of the values of the displacement and stress at the nodes. Then the new unknowns will be the field variables at the nodes. By solving the field equations, these unknowns will be found. Consequently, the field variables can be defined by the approximating functions throughout the assemblage of elements. This is the main idea of FEM.

1.6 Aerobar Used in This Project

This project will focus on the design and evaluation of three shapes of aerobars. The aerobar consist of two parts, one is called aerobar bar-end, which has three different shapes. The other part is called aerobar extension, which is the extended part of the handlebar. The aerobar bar-ends can be removed easily from the aerobar extension.

1.7 Introduction to Testing

In order to verify the FEA result, some sample Mantis bars are built and tested. The Mantis is chosen because it is the easiest bar to fabricate.

The test utilizes the existing test device for the composite fork test of the bicycle [10]. Because the test facility for the twist load is complicated, Mantis was only tested under downward and inward loads.

The test results are plotted in graphs of displacement versus force, thus the stiffness can be obtained using a linear best fit.

Chapter 2: Literature Review

2.1 Some Research Conclusions Concerning Aerobars

Bicyclist experience wind resistance all the time when they are cycling. Wind resistance is caused by two main types of forces: one normal to the front surface of the body, and the other tangential to the surface.

The drag force is approximately proportional to the square of the velocity, so the power to overcome the drag is approximately proportional to the cube of the velocity [11].

Wind tunnel experiments can yield good data for motor vehicles [12], the interaction of the air flow around the cyclist with the "moving" ground is more important, this makes the wind-tunnel data on cyclists less validity than on motors [11].

Lucas Pereira at Stanford University, USA did some measurements on the effect of an aerobar and concluded that aerobars reduce air drag by roughly 20%, which means that the rider can cruise at the same speed with 20% less effort, or ride 8% faster for the same effort [13].

During the racing, air drag accounts for over 90% of the total mechanical resistance to the bicycle [14].

The most effective way to reduce the drag in cycling is to reduce the drag of the cyclist, because the cyclist is responsible for 70% of the air drag [15].

When racing in the wind, if the wind is in proper direction, the aerodynamic components of the bicycle can act as sails and help to reduce air drag [16].

Clip-on aerodynamic handlebars can cut over 1/2 pound from a rider's drag at 30 MPH compared to using the normal bars [17].

2.2 Literature Review on Handlebars/Aerobars

As cycling is an important sport, and the bicycle is not only a transportation tool, the aerodynamic property of a bicycle becomes more and more important. Currently, more and more people are involved in aerodynamic research work on bicycles. Besides trying to make the bicycle as light as possible, by changing the material from steel to composite material, people also try to change the traditional configuration of bicycle.

8

Research work is not only on the bicycle itself, but the posture of the rider is also studied due to the big air drag on a traditional racing bicycle. Aerodynamic handlebars become one of the most effective ways to reduce the air drag during the race. Different shapes of aerobars were designed and fabricated by bicycle companies and amateurs.

The design of an aerobar involves three major aspects: the shape, the material and the attachment method to the other components of the bicycle. Usually the aerobar is fixed to the handlebar.

The following aerobar pictures show some of the most common designs of aerobars in the industry currently [18-25].
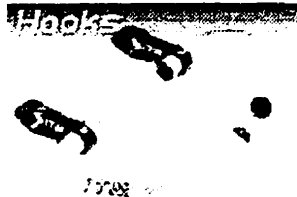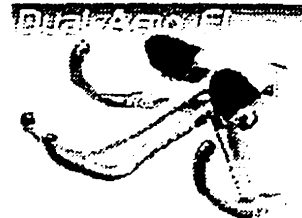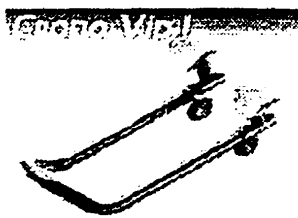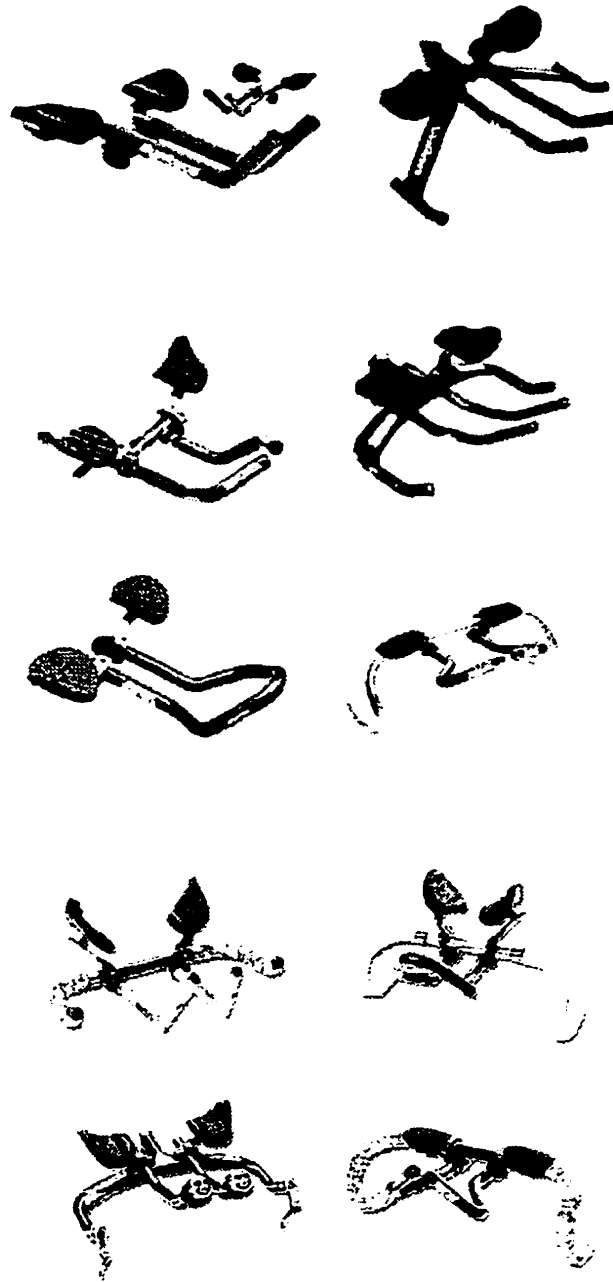
Figure 2.1 Aerobar Configurations in Industry

From the pictures, the shapes of the handlebars are basically the same as traditional handlebars. For the aerobar, if the rider put his hands on it, the hands and arms should create a "nose", like the head of an airplane. So the hands should be very close

each other. As a result, the basic configurations of the aerobars are very similar; two metal tubes extending out from handlebar with either closed end or open end. Two armrests are also included for ergonomic considerations. The distance between the two armrests is adjustable for precise fit, and the armrests can rotate on the mount to find the right position. The length of the aerobar is also adjustable to fit different riders.

The material for the aerobar in industry is aluminum alloy, mostly. Aluminum alloy has relative high strength, low density and cost. These properties make it a better and most popular choice in bicycle industry.

There are a few products that use carbon fiber or titanium as the material for the aerobar. Titanium has higher strength and stiffness than aluminum. Carbon fiber becomes more and more popular in industry due to its outstanding mechanical properties compared with metals and the reduction of its cost in recent years. It is replacing metals and becoming a popular material choice in various sports apparatus.

The aerobar usually clips on to handlebar; this is the most widely used method. This gives it more flexibility than a permanent connection, and it is an easier way to attach it.

2.3 Literature Review on Current Handlebar/Aerobar Designs

The aerobars currently designed almost always include two parts, i.e. aerobar bar-ends and the extended part of the handlebar, which is called aerobar extension for simplicity. These two parts together compose the aerobar.

Different from the materials used in current aerobars, the aerobar designed in this project uses composite material and plastics. The main gain from using composite material is high strength and stiffness, and lightweight. Use of plastics instead of aluminum alloy will reduce the cost in low stress regions.

There are three models of aerobar bar-ends, which were designed by four other students in their course project [26]. They are the Mantis (Figure 2.2), the Claw (Figure 2.3) and the Vader (Figure 2.4). These designs were made to accommodate different types of riders' hand positions.

11
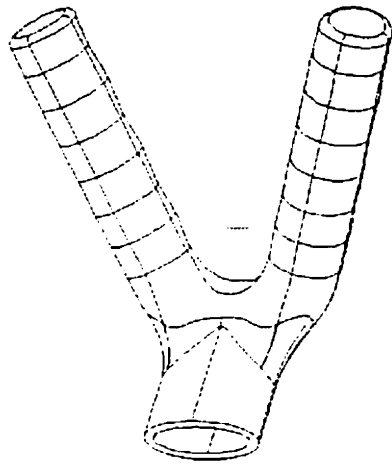
Figure 2.2: Mantis Bar-end
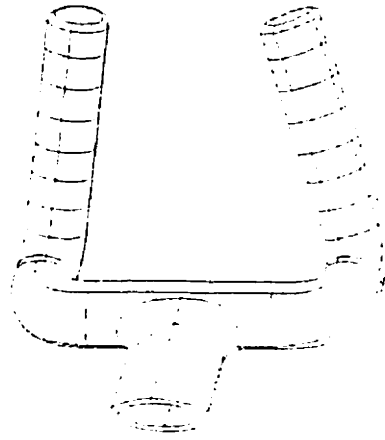
Figure 2.3: Claw Bar-end
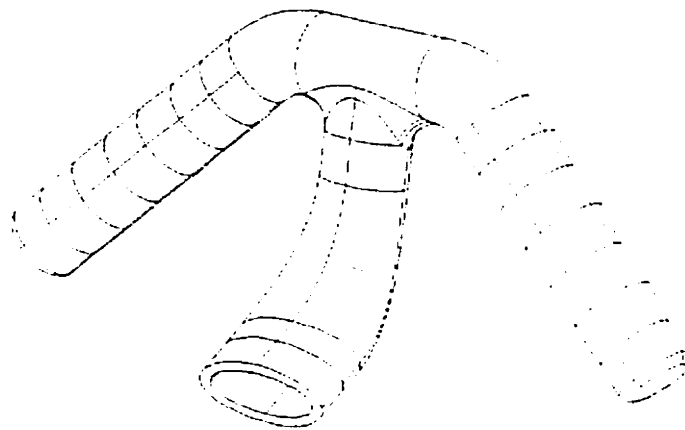
Figure 2.4: Vader Bar-end

All the interface parts of the aerobar bar-ends use elliptical cross-sections, in order to maintain continuity with the aerobar extension, and keep the joint area aesthetically pleasing.

The grips of the aerobar bar-end have cylindrical profiles; there are finger contours on each of the grips, which make the aerobar bar-end more comfortable and easier to hold.

A pair of aluminum plugs, shown in the following figures, is used to join the aerobar extension and aerobar bar-end together. The plug consists of two parts, one female and one male. One of them will be permanently bonded to the aerobar extension, the other to aerobar bar-end, by epoxy. The female and male parts are joined by a setscrew, which makes the attachment or removal of the aerobar bar-end very easy.
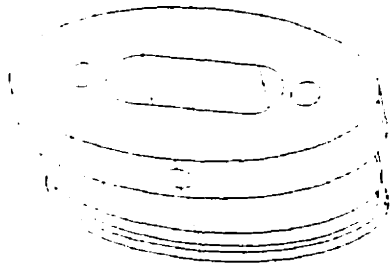
Figure 2.5 Female Plug   **Figure 2.6 Male Plug**
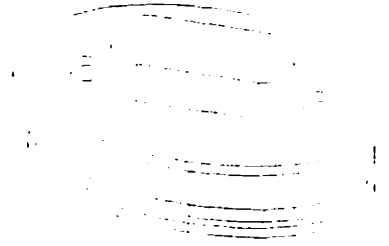
In order to reduce weight, the aerobar bar-end and the plug are all hollowed pieces. There are two holes in the two parts of the plug, which are used to feed the shift cable.

2.4 Literature Review on Materials for the Aerobar

For certain designs, material selection is very important. Consideration of materials and their processing methods start from the early stages of a design. There are three candidate materials for the aerobars: carbon fiber, aluminum alloy and plastic.

Carbon fibers are commonly used composite materials in various fields because of their very good mechanical properties and lightweight at the same time. In this project, carbon fiber is the main material for the bicycle, thus all the critical parts, like the frame. fork and handlebar will be made from carbon fiber. The aerobar extension will be made with woven prepreg LTM25/CF0511, which is a woven carbon fiber that has the following properties [27].

Property	
Fiber Direction Modulus (GPa)	65.6
Matrix Direction Modulus (GPa)	65.6
Shear Modulus (GPa)	3.17
Poisson's Ratio	0.03
Fiber Tensile Strength (MPa)	562
Fiber Compression Strength (MPa)	405
Matrix Tensile Strength (MPa)	562
Matrix Compression Strength (MPa)	405
Shear Strength (MPa)	78.2
Area Density (Kg/m^2)	0.435
Ply Thickness (mm)	0.28
Cost (US$)	$33/Kg

Table 2.1 Mechanical Properties of woven prepreg LTM25/CF0511

Currently, the main material for aerobars in industry is aluminum alloy. This metal has relatively high strength and stiffness compared to plastic, but with high cost and heavy in weight.

For aerobar bar-end, carbon fiber is certainly a good choice considering the mechanical properties and density. However, the cost is much higher than using the aluminum alloy and plastic. On the other hand, carbon fiber is difficult to use in parts with small curvature radius like the Claw and the Vader bar. If metal or plastic is the chosen material, and considering the design of aerobar bar-ends, casting or injection molding are the appropriate processing methods.

Notice that the aerobar bar-end is a small part of a composite bicycle; it should be as light as possible, and the cost should be low. The shape of the part is also quite complex. All these make plastic a better choice than metal.

The nature of plastics can be divided into two major classifications: thermosetting materials and thermoplastic materials. Thermosetting plastics are cured into a permanent shape, while thermoplastic, when heated, will become soft or melt to a flowable state

[28]. Acrylonitrile Butadiene Styrene (ABS) is a commonly used thermoplastic. One of the outstanding mechanical properties of ABS is impact resistance. When impact failure occurs, it will be ductile rather than brittle. ABS has a good balance of strength, hardness, density and cost. Moreover, it is easy to use with injection fabrication processes. All these properties make ABS a good choice for the aerobar bar-ends. The main properties for a typical ABS (molded) are listed below [29].

Property	
Density (g/cm^3)	1.05
Linear Mold Shrinkage (cm/cm)	0.0064
Melt Flow (g/10 min)	9.3
Tensile Strength, Yield (MPa)	44.8
Modulus of Elasticity (GPa)	2.4
Compressive Yield Strength (MPa)	64
Poisson's Ratio	0.38

Table 2.2 Mechanical Properties of ABS, Molded

Chapter 3: Finite Element Analysis on the Aerobars

The aerobar of a bicycle has to be able to withstand the maximum load applied due to competitive cycling. In order to know if the design and the material used can satisfy this basic requirement, we have to perform the necessary analysis. FEM software named I-DEAS is used.

3.1 Structure Description:

The whole structure examined in the Finite Element Analysis includes two parts: aerobar bar-ends and the extended part of the handlebar, which is called aerobar extension, for simplicity. These two parts together compose the aerobar.

All the three aerobar bar-ends have to be fixed on the extended part of the handlebar (aerobar extension), which has the shape shown below.
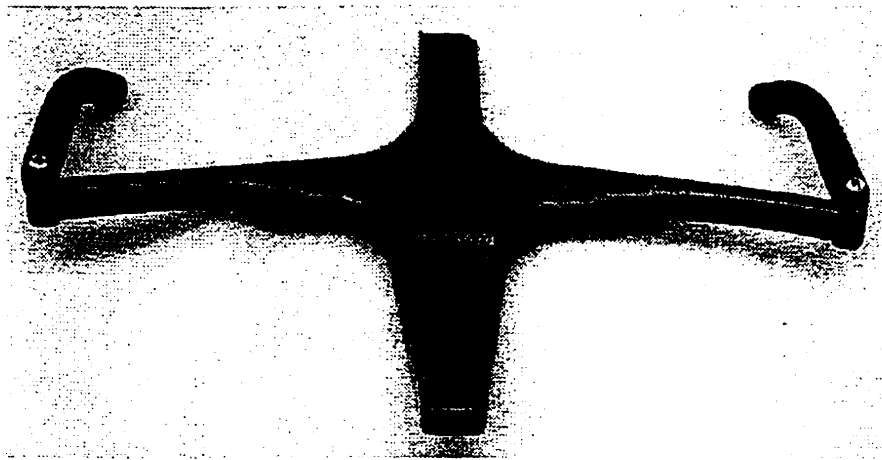
Figure 3.1   Handlebar

The finite Element Analysis performed in this project includes the aerobar extension and the aerobar bar-ends, which are shown below with the Mantis as an example.
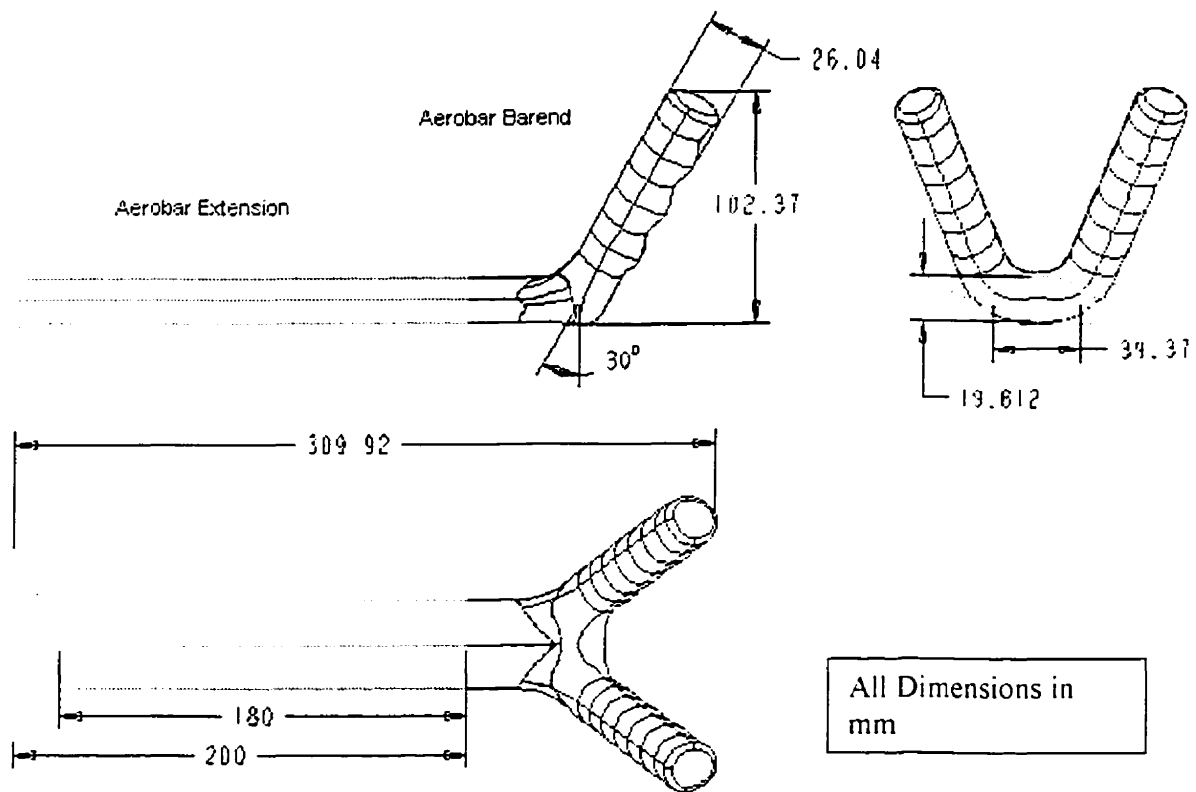
Figure 3.2 Basic Structures for FEM Analysis

3.2 Finite Element Model Description

3.2.1 Mesh:

The geometry of the whole aerobar is imported together, i.e. assemble the aerobar bar-ends with the aerobar extension in Pro_E software, create an IGES file, and then import to I-DEAS. I-DEAS treats the bar-ends and the extension as a whole geometry with many surfaces, the two parts connected to each other as one piece, therefore, and it is not necessary to put constraints between them. Even so, to prevent possible errors. the aerobar bar-ends and the extension are meshed separately.

Because the entire bar is a hollow structure, and considering the ratio of the thickness to the other dimensions of the bar, the thin shell element is the appropriate choice. In this project, the Finite Element Analysis uses the "thin shell parabolic triangle element". This is a curved triangle element; it is better than the plane triangular element

for modeling curved surfaces. The element length is space10, which means that the side length of the typical triangle is approximately10mm.

3.2.2 Boundary Conditions:

Because the handlebar is made of Carbon Fiber, which has very high stiffness, the displacement is very small in the joint area when put load on aerobar bar-end, so the joint area can be considered as clamped, i.e. fully constrained, for the extended part of the handlebar. The figure below shows the clamped end using the Mantis as an example.

Clamped End
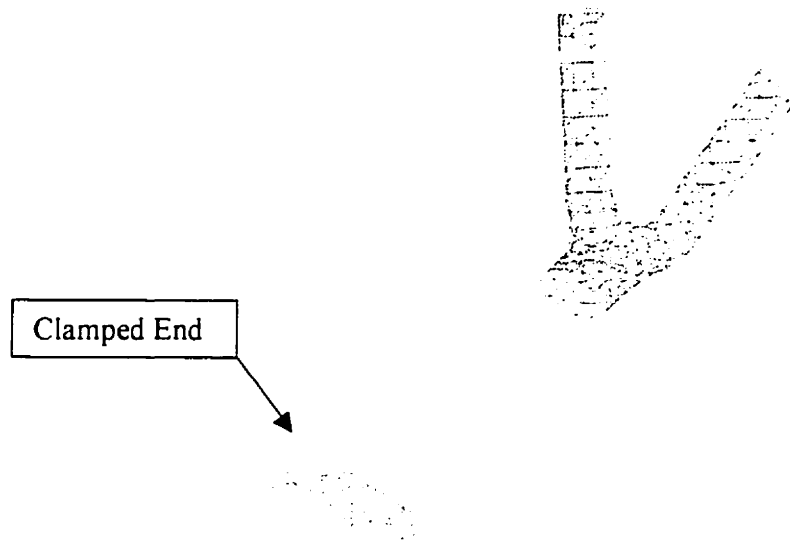
Figure 3.3 Boundary Condition Illustrations

3.2.3 Load Description

There are three kinds of static load cases: downward load, inward load and the twist load. These loads are to simulate the real loads that a bicycle could withstand in normal competitive cycling. These load cases were not derived from the literature but were assumed intuitively from an analysis of possible loads that one can subject to a bicycle during heavy use.

Downward load:

In this case, 50Kg force, which is perpendicular to the ground, is put on each grip of the aerobar bar-end, so the total load will be 100Kg. This load is from the rider due to putting all the body weight on the aerobar. Generally, a rider's body weight will not exceed 100Kg. The static response of the aerobar under this load is predicted in this case. The downward load will be put on each grips of the aerobar bar-end.

For the Mantis and the Claw, there are 12 surfaces on each grip. In I-Deas, total force on each surface is needed, which is the following:

Total force on each surface   = 100 (Kg)/24

                               = 4.1667 (Kg)

                               = 40.8333 (Newton)

For the Vader, a total of 12 surfaces are used for the downward load, thus the force on each surface is:

Total force on each surface   = 100 (Kg)/12

                               = 8.3334 (Kg)

                               = 81.6667 (Newton)

Inward Load:

In this case, a total of 100Kg force is applied to the aerobar bar-end opposite to the direction of riding. The purpose of this load case is to simulate the impact effect when the bicycle crashes. The simulation is simplified by replacing impact loads with static ones.

The inward load will be put on the ends of the grips for the Mantis and the Claw. On each end, the total force will be 50 Kg, i.e. 490 N. For the Vader, the total 100 Kg load will be put on the front part furthest away from the rider.

Twist Load:

In this case, 50Kg force perpendicular to the ground is put on each grip of the aerobar bar-end, so the total load will be 100Kg. The difference between this case and the

downward case is that the directions for the two 50Kg forces in the twist case are opposite to each other, creating a moment or "twisting load". This can occur when the rider is pedaling heavily (such as climbing a hill or accelerating).

As in the downward load case, the twist load will also be put on the grips of the aerobar; and the total force on each grip is 40.8333N.

3.3 Convergence Study

The Finite Element Method is a numerical technique, thus the results from a FEM is an approximate solution of the problem. The more the elements used, in other words, the smaller the element size, and the better the result. Theoretically, the result will converge to the exact solution as the number of element increases.

Mathematically, there are some conditions that the interpolation polynomials must satisfy in order to ensure convergence, as follow [30].

1) If one chooses continuous functions as interpolation functions, the field variable will be continuous within the element.

2) The assumed displacement model must permit rigid body motion and constant strain states of the element.

3) At element boundaries or interfaces, the field variable and its partial derivatives up to one order less than the highest order derivative must be continuous.

In the case of general solid and structural mechanics problems, these requirements mean that the adjacent elements must deform without causing openings, overlaps or discontinuities.

If the interpolation polynomial satisfies all the three requirements, the approximate solution converges to the correct solution when we refine the mesh and use an increasing number of smaller elements. Valid interpolation functions are used in this project by the choice of "thin shell parabolic triangle elements" in the FEM. Thus, it remains to determine if the number of elements used is adequate.

In this project, using the Mantis bar as an example, the maximum and minimum stress values are used to study the convergence.

Load:

The FEM analysis is performed using load case 1, i.e. downward load, with a distributed load on each grip, the total load on the bar is 100Kg.

Element:

The aerobar is meshed with three different element lengths, i.e. 15, 10 and 5. Due to the curved surfaces and the dimension of the structure, thin shell parabolic triangle elements are chosen to perform the convergence study. Table 3.1 shows a summary of elements and nodes used in the three models.

Model	Number of Node	Number of Element
El. Length 15	3253	1606
El. Length 10	3573	1752
El. Length 5	8764	4362

Table 3.1 Elements and Nodes in the Models

Boundary Condition:

As stated in section 3.2.2, the end of the aerobar extension is a clamped boundary condition.

The meshed model with boundary conditions is shown below:
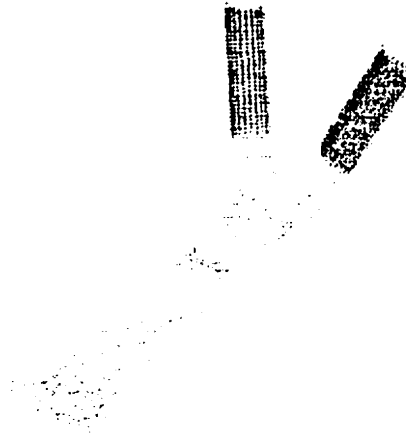
Figure 3.4 Mantis Bar, Meshed model, Downward Load

Analysis Results

The maximum and minimum stresses in the Aerobar meshed with different element lengths are listed in Table 3.2.

Unit: 10^3Pa

	Aerobar extension		Aerobar bar-end	
	σmax	σmin	σmax	σmin
El. Length 15	2.445e5	-2.84e4	6.69e4	-2.467e4
El. Length 10	2.511e5	-2.752e4	6.75e4	-2.492e4
El. Length 5	2.678e5	-2.821e4	6.647e4	-2.576e4

Table 3.2 Stresses Used in Convergence Study

Conclusion:

From the analysis results, we see that the stress values in the three cases are very close, thus the results are converged. In the following analysis, we choose the element length 10 to mesh the model.

3.4 Finite Element Analysis Results for All Aerobars:

Load:

22

Although the total force on each bar in each case is the same, the area on which the distributed load applied is different. For this reason, the load cases will be explained individually for each aerobar.

Mesh:

Element Type: Higher order triangular thin shell element

Element Length: 10 for both aerobar bar-end and aerobar extension.

The following table summarized the number of nodes and elements of the three aerobar meshing.

Model	Number of Node	Number of Element
Mantis	3573	1752
Claw	4501	2228
Vader	4353	2132

Table 3.3 Mesh Result of Aerobars

Thickness of element:

Aerobar Bar-end: 3mm everywhere.

Aerobar Extension: 2mm for most of the part. Near the clamped end, the thickness becomes 4mm and 6mm, to simulate the reality of manufacturing.

Boundary Condition:

Clamped at the end of aerobar extension. (See section 3.2.2)

Failure Criteria:

The Maximum Principle Stress Criteria is used as a failure criterion to examine the stress levels. Because of the fairly simple nature of the loading, the structures tended to be in pure bending (or torsion) and the maximum stresses were nearly always in the long direction of the aerobars. Verifications were made, showing that the direction of the maximum principle stress and the longitudinal (Z-direction) direction nearly always coincided. Therefore, using the maximum principal stress criterion is justified.

23

3.4.1 Mantis bar:

3.4.1.1 Load Case 1: Downward load

Load:

Total force: 50Kg X 2 on each model, i.e. 40.8333N on each surface of 24 surfaces.

Direction: -Y direction of the default coordinate system in FEM model. This direction is perpendicular to aerobar extension and towards the ground.
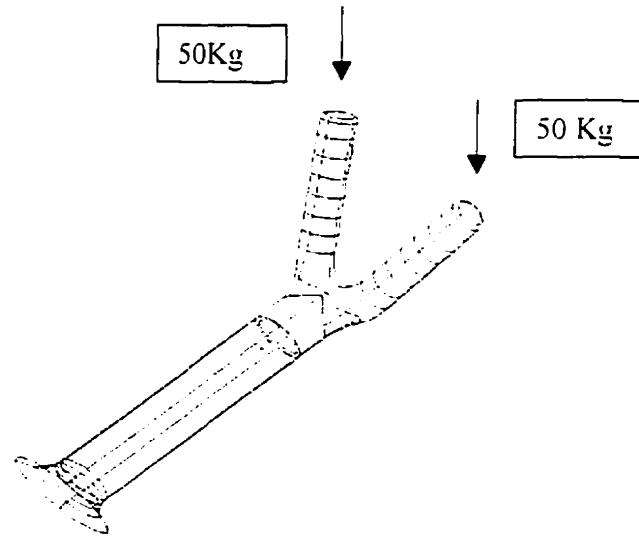
Figure 3.5 FEM Model for Mantis, Downward Load

Stress Results:

The stress distribution contours for this case are shown in Figure 3.6, the numbers in the boxes are the node numbers of the maximum and minimum stress by using Maximum Principle Stress criteria.

The table that follows (Table 3.5) lists the maximum principle stress, maximum shear stress and the Von Mises stress values for this load case, and the node numbers corresponding to these stress values are also listed.

VALUE OPTION:ACTUAL
SHELL SURFACE: TOP

2.51E+05
2.23E+05
1.95E+05
1.67E+05
1.40E+05
1.12E+05
8.39E+04
5.61E+04
2.82E+04
3.40E+02
-2.75E+04

1300

2597

VALUE OPTION:ACTUAL
SHELL SURFACE: TOP

3.51E+05
3.23E+05
1.95E+05
1.67E+05
1.40E+05
1.12E+05
8.39E+04
5.61E+04
2.82E+04
3.40E+02
-2.75E+04

67

2073

Front View   Back View
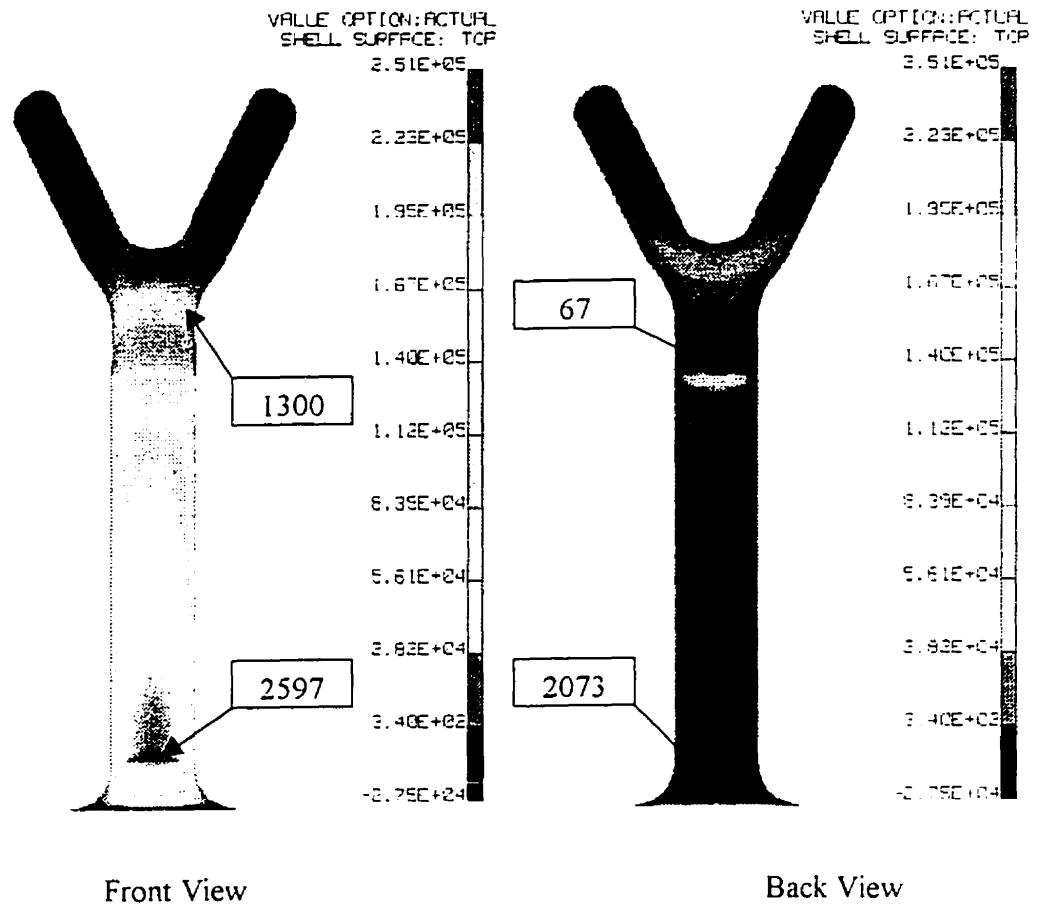
Figure 3.6 Stress Distribution for Mantis, Downward Load

		Max. Prin.	Max. Shear	Von Mises
Aerobar Bar-end	Node	1300	67	67
	σmax	6.75e4	3.87e4	6.843e4
	Node	67	1737	1737
	σmin	-2.492e4	13.21	24.57
Aerobar Extension	Node	2597	3181	2111
	σmax	2.511e5	1.256e5	2.420e5
	Node	2073	1892	1892
	σmin	-2.752e4	1.536e2	2.922e2

Table 3.4 Stress Results for Mantis, Downward Load

The following table shows the maximum and minimum node displacements for this load case. The "Disp-X", "Disp-Y" and "Disp-Z" mean the node displacements along X, Y and Z axes, respectively. The "Disp-RX", "Disp-RY" and "Disp-RZ" refer to the rotation angles around X, Y and Z axes. The unit for displacement is mm, for rotation is radian. The maximum displacement magnitude is also listed; "M.D.M." in the table stands for this value.

	Disp-X (mm)	Disp-Y (mm)	Disp-Z (mm)	Disp-RX (rad)	Disp-RY (rad)	Disp-RZ (rad)	M.D.M. (mm)
Node	1793	2170	316	2214	40	404	
Maximum	0.77588	7.725e-03	1.24	1.037e-03	3.318e-2	6.02e-02	
Node	713	134	714	1287	399	427	23.8
Minimum	-0.816	-20.3	-14.23	-0.1861	-3.356e-2	-5.86e-2	

Table 3.5 Maximum and Minimum Node Displacements for Mantis, Downward Load

Discussion:

From the FEA results, for the aerobar bar-end, the maximum tensile stress appears to be on the upper part of the elliptical section; the maximum compression stress appears to be on the lower part of the same section. In the back view, there are two tensile stress areas; this is stress concentration due to the change of geometry, the material and the thickness.

For the aerobar extension, the maximum tensile stress is near the upper part of the clamped area. There is a sudden change of stress in this area; this is due to the sudden change of the thickness in the model, i.e. from 2mm in most of the elements to 4mm and 6mm near the end. In reality, the thickness of aerobar extension will change gradually, thus this stress gap will not appear.

The maximum compression stress in the aerobar extension appears to be on the lower part of the clamped area. There is also a sudden compression stress change on this part of the bar due to the same reason as in tensile stress.

3.4.1.2 Load Case 2: Inward load

Load:

Total force: 50Kg X 2 on each model, i.e. 490N on each of the 2 surfaces.

Direction: Z direction of the default coordinate system in FEM model. This direction is parallel to the ground and the aerobar extension, and opposite to the riding direction.
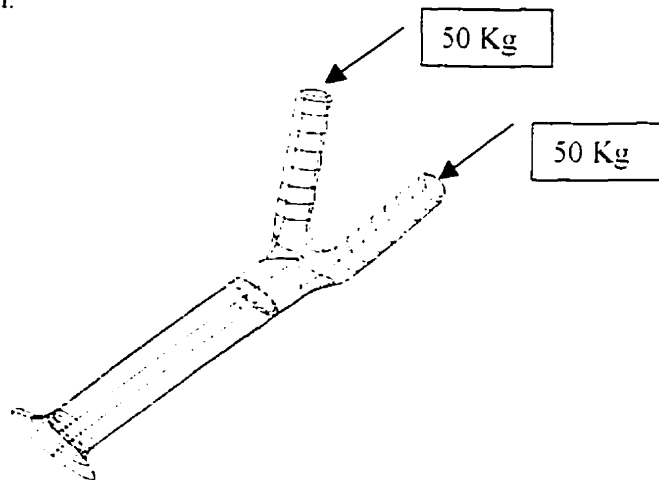
Figure 3.7 FEM Model for Mantis. Inward Load

Stress Results:

The stress distribution contours for this case are shown in Figure 3.8, the numbers in the boxes are the node numbers of the maximum and minimum stress by using Maximum Principle Stress criteria.

The table that follows (Table 3.6) lists the maximum principle stress, maximum shear stress and the Von Mises stress values for this load case, and the node numbers corresponding to these stress values are also listed.

Front view   Back view
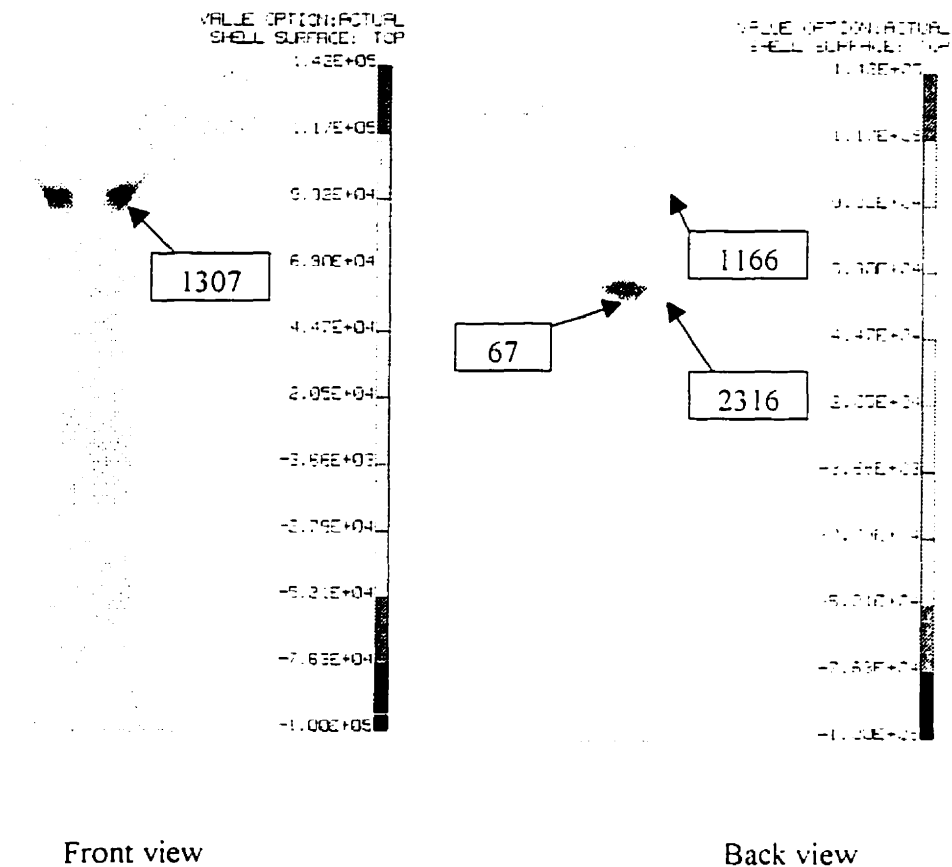
Figure 3.8 Stress Distribution for Mantis, Inward Load

		Max. Prin.	Max. Shear	Von Mises
Aerobar bar-end	Node	1166	1300	1300
	σmax	9.254e4	6.884e4	1.216e5
	Node	1307	1758	1758
	σmin	-1.005e5	4.332e2	8.315e2
Handle-bar	Node	67	67	67
	σmax	1.556e5	1.093e5	1.95e5
	Node	2316	1890	1890
	σmin	-1.425e4	35.32	61.29

Table 3.6 Stress Results for Mantis, Inward Load

The following table (Table 3.7) shows the maximum and minimum node displacements for this load case. The maximum displacement magnitude is also listed; "M.D.M." in the table stands for this value.

	Disp-X (mm)	Disp-Y (mm)	Disp-Z (mm)	Disp-RX (rad)	Disp-RY (rad)	Disp-RZ (rad)	M.D.M. (mm)
Node	1789	693	1793	1287	1309	1171	
Maximum	6.993	22.95	**26.33**	**0.3258**	0.1097	0.1025	
Node	697	2170	316	2214	1501	1149	**33.4**
Minimum	-6.801	-3.052c-3	-1.493	-3.930c-4	-8.899c-2	-9.8c-2	

Table 3.7 Maximum and Minimum Node Displacements for Mantis, Inward Load

Discussion:

From the FEA results, for the aerobar bar-end, the maximum tensile stress appears to be on the joint area of the grips merging with the elliptical section; the maximum compression stress also appears to be in the same area.

In the front view, there is a small higher tensile stress area, and in the back view, there is a small higher compression stress area when the grips join together. These are because the two 50Kg loads create two moments, which are along the ±Y direction in this area. The Y direction is perpendicular to the ground and the aerobar extension.

For the aerobar extension, the maximum tensile stress is near the interface area with the aerobar bar-end. This is the stress concentration due to the change of material and thickness.

There is a sudden change of stress near the clamped area; the reason is the same as stated in the downward load case.

The maximum compression stress in aerobar extension also appears to be near the interface area with the aerobar bar-end. Again, there is sudden compression stress change on aerobar extension.

3.4.1.3 Load Case 3: Twist load

Load:

Total force: 50Kg X 2 on each model, i.e. 40.8333N on each surface of 24 surfaces.

Direction: ±Y direction of the default coordinate system in FEM model. This direction is perpendicular to the ground and aerobar extension.

50 Kg

50 Kg
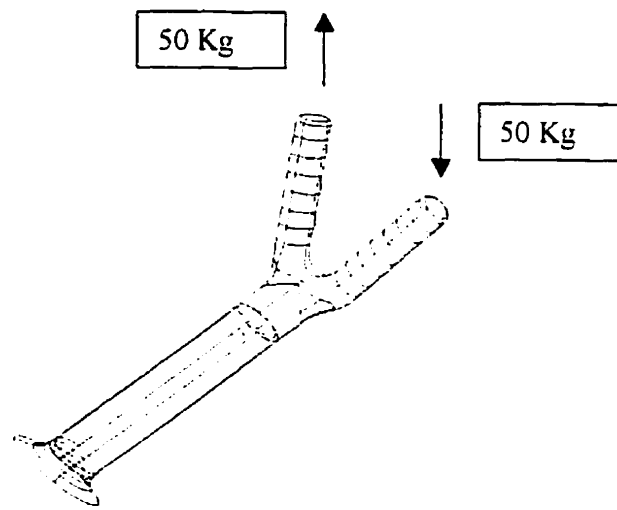
Figure 3.9 FEM Model for Mantis, Twist Load

Stress Results:

The stress distribution contours for this case are shown in Figure 3.10, the numbers in the boxes are the node numbers of the maximum and minimum stress by using Maximum Principle Stress criteria.

The table that follows (Table 3.8) lists the maximum principle stress. maximum shear stress and the Von Mises stress values for this load case. and the node numbers corresponding to these stress values are also listed.

407

1489

438

2230

Front View   Back View
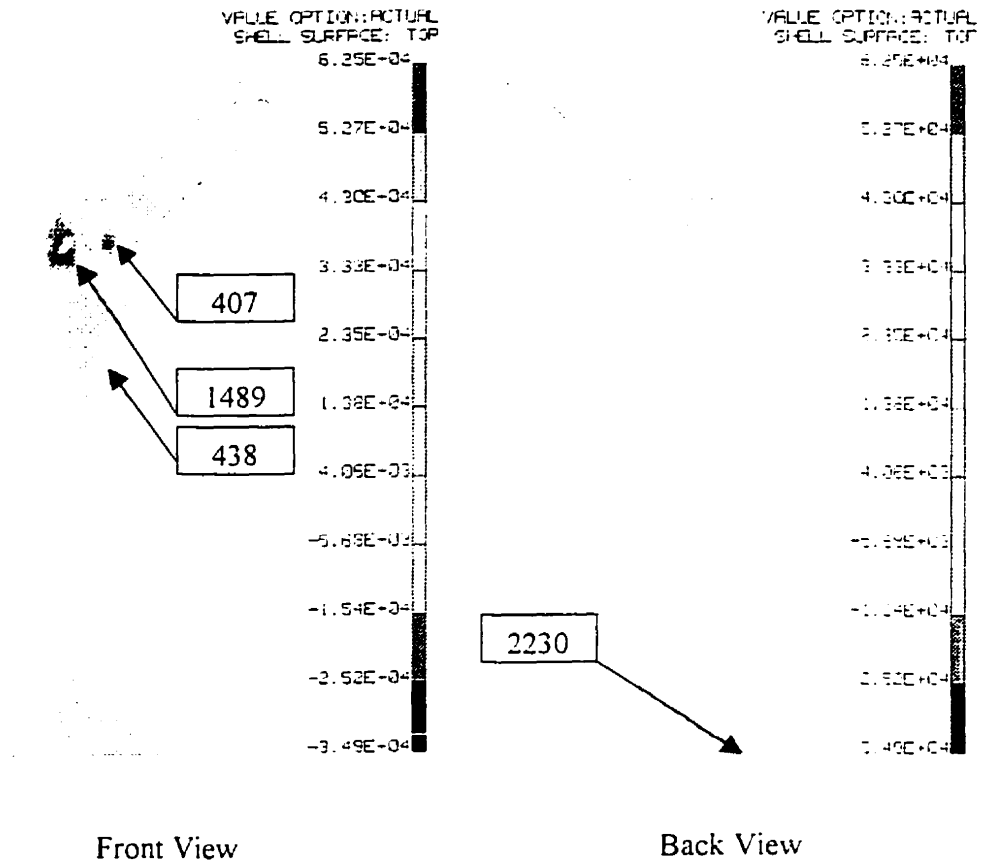
Figure 3.10 Stress Distribution for Mantis, Twist Load

		Max. Prin.	Max. Shear	Von Mises
Aerobar	Node	407	1489	407
bar-end	σmax	6.251e4	3.148e4	5.528e4
	Node	1489	1768	1768
	σmin	-3.49e4	8.445	16.41
Handle-	Node	438	450	450
bar	σmax	2.935e4	2.835e4	4.923e4
	Node	2230	1892	1892
	σmin	-2.213e2	19.47	33.73

Table 3.8 Stress Result for Mantis, Twist Load

The following table (Table 3.9) shows the maximum and minimum node displacements for this load case. The maximum displacement magnitude is also listed; "M.D.M." in the table stands for this value.

	Disp-X (mm)	Disp-Y (mm)	Disp-Z (mm)	Disp-RX (rad)	Disp-RY (rad)	Disp-RZ (rad)	M.D.M.
Node	1796	704	714	982	1309	1324	(mm)
Maximum	7.68	**8.59**	5.771	7.52e-02	4.441e-02	3.331e-02	
Node	1101	1729	1796	1271	1328	1246	11.6
Minimum	-0.6387	-5.336	-1.822	-3.287e-2	-5.069e-2	-0.1026	

Table 3.9 Maximum and Minimum Node Displacements for Mantis, Twist Load

Discussion:

From the FEA results, for the aerobar bar-end, the maximum tensile stress appears to be on the joint area of the grips merging with the elliptical section; the maximum compression stress also appears to be in the same area.

For the aerobar extension, the stress is almost the same everywhere, because it undergoes a pure twist load.

3.4.1.4 Summary of Maximum Stress for Mantis:

Unit: 10^3Pa

	Aerobar extension		Aerobar bar-end	
	σmax	σmin	σmax	σmin
Load Case 1	**2.511e5**	**-2.752e4**	6.75e4	-2.492e4
Load Case 2	1.556e5	-1.425e4	**9.254e4**	**-1.005e5**
Load Case 3	2.935e4	-2.213e2	6.251e4	-3.49e4

Table 3.10 Maximum Stress Summary of Mantis

From the above table, we see that for aerobar bar-end, inward load case is the worst case, maximum stress for both tensile and compression is the biggest among the three load cases. Therefor, the ability to withstand the impact load is critical for the Mantis bar. Increasing the radius of the round corner will improve its resistance to impact loads.

For the aerobar extension, downward load is the worst case, maximum stress for both tensile and compression is the biggest among the three load cases. The design should mainly consider the rider's body weight.

3.4.2 Claw bar:

3.4.2.1 Load Case 1: Downward load

Load:

> *Total force:* 50Kg X 2 on each model, i.e. 40.8333N on each of 24 surfaces.
>
> *Direction:* -Y direction of the default coordinate system in FEM model. This direction is perpendicular to the aerobar extension and towards the ground.

Figure 3.11 FEM Model for Claw, Downward Load

Stress Results:

The stress distribution contours for this case are shown in Figure 3.12, the numbers in the boxes are the node numbers of the maximum and minimum stress by using Maximum Principle Stress criteria.

The table that follows lists the maximum principle stress, maximum shear stress and the Von Mises stress values for this load case, and the node numbers corresponding to these stress values are also listed.
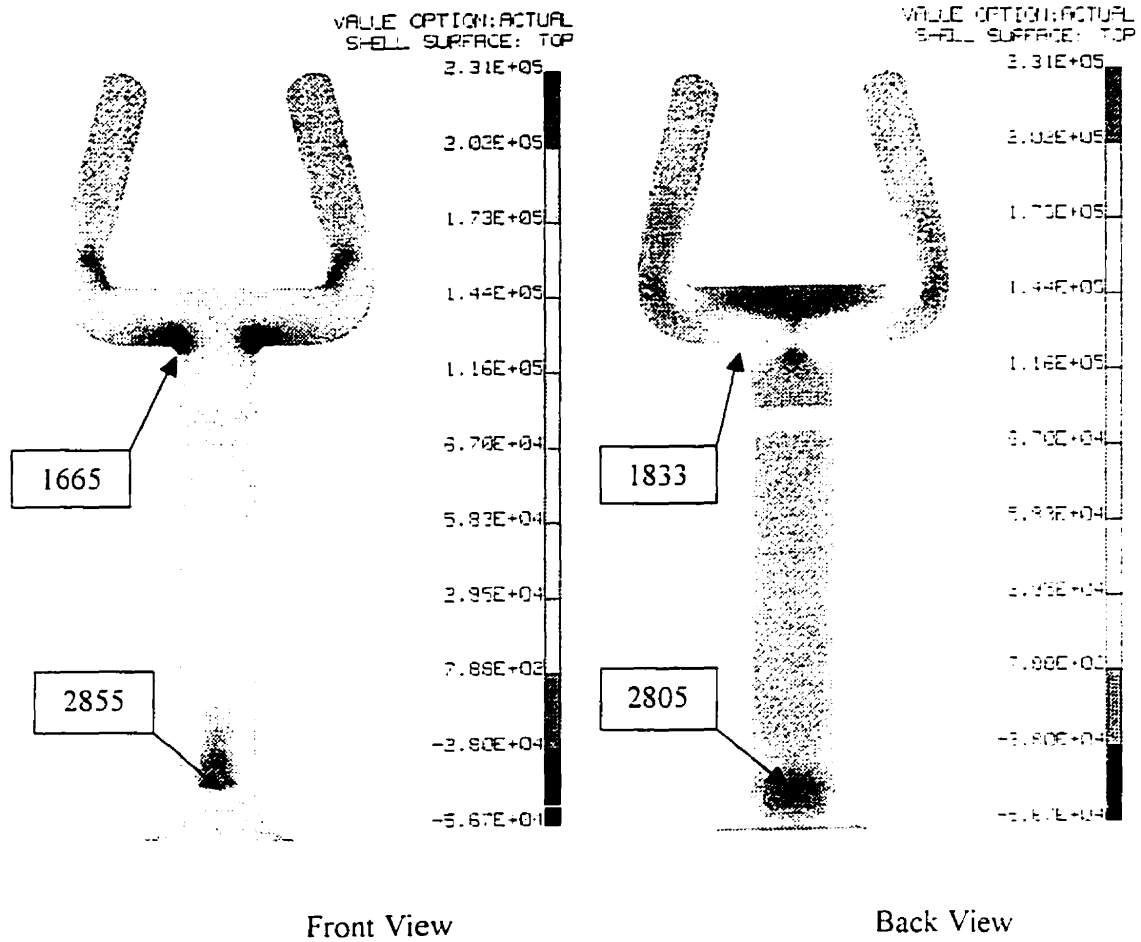
Figure 3.12 Stress Distribution for Claw, Downward Load

		Max. Prin.	Max. Shear	Von Mises
Aerobar	Node	1833	1665	1665
bar-end	σmax	1.206e5	6.058e4	1.049e5
	Node	1665	1188	1188
	σmin	-5.878e4	88.92	1.606e2
Handle-	Node	2855	3028	3028
bar	σmax	2.307e5	1.153e5	2.265e5
	Node	2805	2820	2820
	σmin	-3.029e4	1.297e2	2.277e2

Table 3.11 Stress Result for Claw, Downward Load

The following table (Table 3.12) shows the maximum and minimum node displacements for this load case. The maximum displacement magnitude is also listed; "M.D.M." in the table stands for this value.

	Disp-X (mm)	Disp-Y (mm)	Disp-Z (mm)	Disp-RX (rad)	Disp-RY (rad)	Disp-RZ (rad)	M.D.M. (mm)
Node	259	3107	1289	3155	1635	1979	
Maximum	0.5342	8.652e-03	3.408	1.157e-03	0.114	7.644e-02	
Node	187	1227	212	493	1917	1842	49.4
Minimum	-0.5511	-44.15	-26.73	-0.3658	-7.419e-2	-7.35e-2	

Table 3.12 Maximum and Minimum Node Displacements for Claw, Downward Load

Discussion:

Both the maximum tensile and compression stress on the aerobar bar-end are in the corner of the T-shaped area, and the stresses in these two small areas are much higher than in other areas. Changing the radius of the round corner, and making a smoother

transition will improve the situation. Stress concentrations also appear in the sharp corner when the grips connect to the T-shaped part. This area also needs to be modified in the design.

The stress condition on the aerobar extension is similar to that in the Mantis under the downward load.

There is also a stress concentration in the joint area of the bar-end and the extension due to the change of the material and the thickness.

3.4.2.2 Load Case 2: Inward load

Load:

Total force: 50Kg X 2 on each model, i.e. 490N on each surface of 2 surfaces.

Direction: Z direction of the default coordinate system in FEM model. This direction is parallel to the ground and the aerobar extension, and opposite to the riding direction.
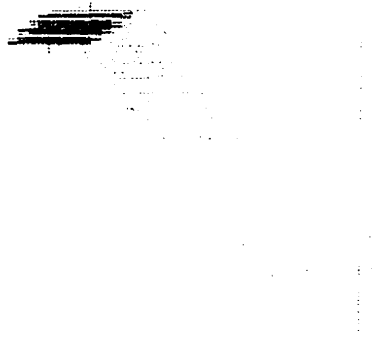
Figure 3.13 FEM Model for Claw, Inward Load

Stress Results:

The stress distribution contours for this case are shown in Figure 3.14, the numbers in the boxes are the node numbers of the maximum and minimum stress by using Maximum Principle Stress criteria.

The table that follows (Table 3.13) lists the maximum principle stress, maximum shear stress and the Von Mises stress values for this load case, and the node numbers corresponding to these stress values are also listed.

Front View   Back View
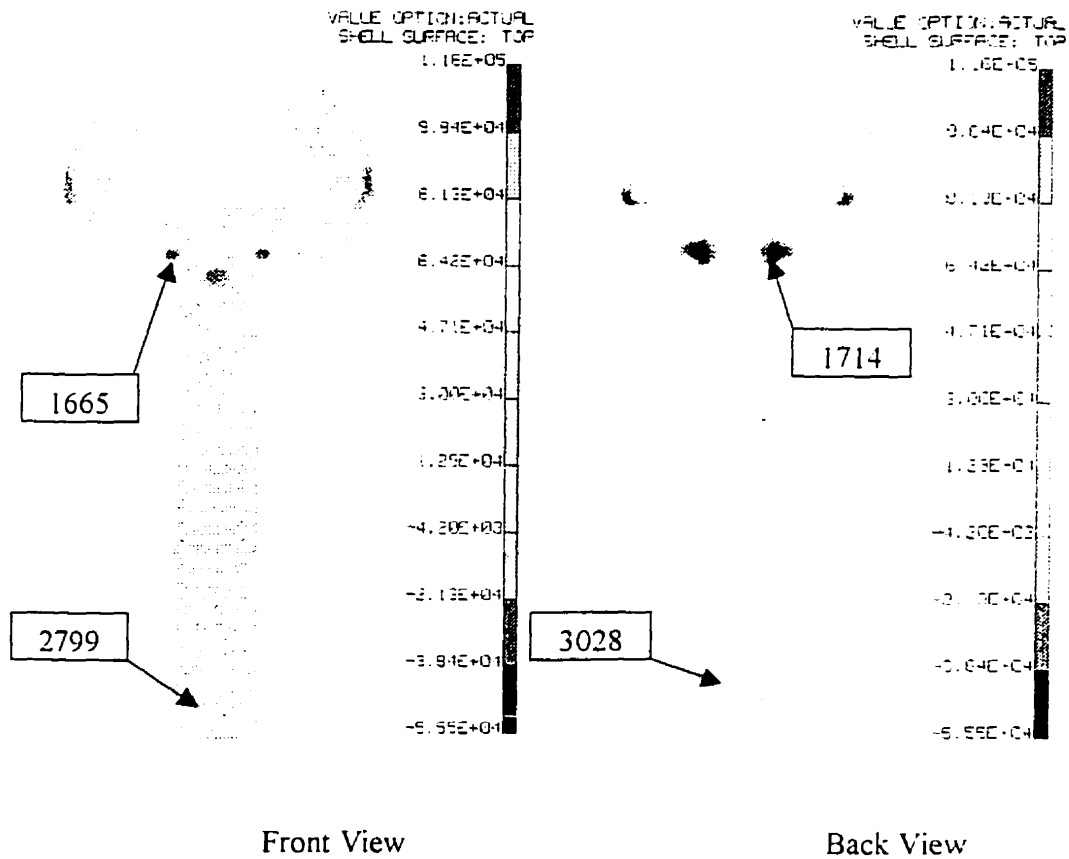
Figure 3.14 Stress Distribution for Claw, Inward Load

		Max. Prin.	Max. Shear	Von Mises
Aerobar bar-end	Node	1665	1833	1833
	σmax	1.166e5	5.841e4	1.013e5
	Node	1714	173	173
	σmin	-5.741e4	3.271e2	6.233e2
Aerobar Extension	Node	3028	409	2827
	σmax	5.739e4	3.493e4	6.701e4
	Node	2799	3173	3173
	σmin	-8.146e3	1.029e2	1.886e2

Table 3.13 Stress Result for Claw, Inward Load

The following table shows the maximum and minimum node displacements for this load case. The maximum displacement magnitude is also listed; "M.D.M." in the table stands for this value.

	Disp-X (mm)	Disp-Y (mm)	Disp-Z (mm)	Disp-RX (rad)	Disp-RY (rad)	Disp-RZ (rad)	M.D.M. (mm)
Node	370	1227	212	2706	1339	830	
Maximum	2.913	**38.95**	30.83	**0.3902**	6.569e-02	9.336e-2	
Node	1180	3106	1289	3130	1635	2706	46.8
Minimum	-2.896	-2.671e-3	-2.769	-3.438e-4	-0.1132	-9.304e-2	

Table 3.14 Maximum and Minimum Node Displacements for Claw, Inward Load

Discussion:

As in the downward load case, the maximum tensile and compression stresses are also located in the corner of T-shaped area, and there are stress concentrations in the bottom of the grips. The effect of the sharp corner is even worse in this case than it was for the downward load case. Again, there are very high stresses in two small areas.

The equivalent loads on the aerobar extension are bending and compression, so the stress is almost the same along the length direction. There are stress concentrations in the interface area and near the clamped end.

3.4.2.3 Load Case 3: Twist load

Load:

Total force: 50Kg X 2 on each model, i.e. 40.8333N on each surface of 24 surfaces.

*Direction:* ±Y direction of the default coordinate system in FEM model. This direction is perpendicular to the ground and the aerobar extension.
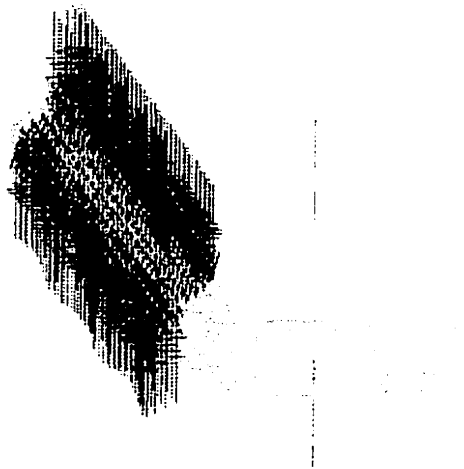
Figure 3.15 FEM Model for Claw, Twist Load

Stress Results:

The stress distribution contours for this case are shown in Figure 3.15, the numbers in the boxes are the node numbers of the maximum and minimum stress by using Maximum Principle Stress criteria.

The table that follows lists the maximum principle stress, maximum shear stress and the Von Mises stress values for this load case, and the node numbers corresponding to these stress values are also listed.

VALUE OPTION:ACTUAL
SHELL SURFACE: TOP

9.27E+04

7.74E+04

6.21E+04

4.67E+04

3.14E+04

1.61E+04

7.81E+03

-1.45E+04

-2.99E+04

-4.52E+04

-6.05E+04

1626

285

3675

Front View

VALUE OPTION:ACTUAL
SHELL SURFACE: TOP

9.27E+04

7.74E+04

6.21E+04

4.67E+04

3.14E+04

1.61E+04

7.81E+03

-1.45E+04

-2.99E+04

-4.52E+04

-6.05E+04

1678

Back View

Figure 3.15 Stress Distribution for Claw, Twist Load

		Max. Prin.	Max. Shear	Von Mises
Aerobar bar-end	Node	1626	1626	1626
	σmax	9.437e4	4.718e4	8.298e4
	Node	1678	352	352
	σmin	-6.237e4	51.56	95.56
Handle-bar	Node	285	5	5
	σmax	5.531e4	4.520e4	7.831e4
	Node	3675	2820	2820
	σmin	-6.407e3	10.84	19.38

Table 3.15 Stress Result for Claw, Twist Load

The following table shows the maximum and minimum node displacements for this load case. The maximum displacement magnitude is also listed; "M.D.M." in the table stands for this value.

	Disp-X (mm)	Disp-Y (mm)	Disp-Z (mm)	Disp-RX (rad)	Disp-RY (rad)	Disp-RZ (rad)	M.D.M. (mm)
Node	212	376	212	2706	2024	405	
Maximum	11.23	**22.1**	15.14	**0.2054**	0.1007	5.976e-02	
Node	2676	1188	1358	830	1982	891	**27.6**
Minimum	-1.555	-15.59	-10.04	-0.1406	-7.623e-2	-0.1914	

Table 3.16 Maximum and Minimum Node Displacements for Claw, Twist Load

Discussion:

Again, the highest stress is in the corners on the bar-end, as in the other two load cases.

On the aerobar extension, because it undertakes pure twist moment, the stress is almost the same everywhere, except the interface area with the bar-end, there is stress concentration there.

3.4.2.4 Summary of FEA Stress Results for Claw:

<div align="right">Unit: 10^3Pa</div>

	Aerobar extension		Aerobar bar-end	
	σmax	σmin	σmax	σmin
Load Case 1	**2.307e5**	**-3.029e4**	**1.206e5**	-5.878e4
Load Case 2	5.739e4	-8.146e3	1.166e5	-5.741e4
Load Case 3	5.531e4	-6.407e3	9.437e4	**-6.237e4**

Table 3.17 Maximum Stress Summary for Claw Bar-end

All the FEA results from the three load cases show that the four sharp corners on the claw have much higher stress than the other parts, thus it is necessary to re-design the dimensions of this part. It will help if the sharp corner is changed into a mild one.

3.4.3 Vader Bar
3.4.3.1 Load Case 1: Downward load
Load:

Total force: 50Kg X 2 on each model, i.e. 81.6667N on each surface of 12 surfaces.

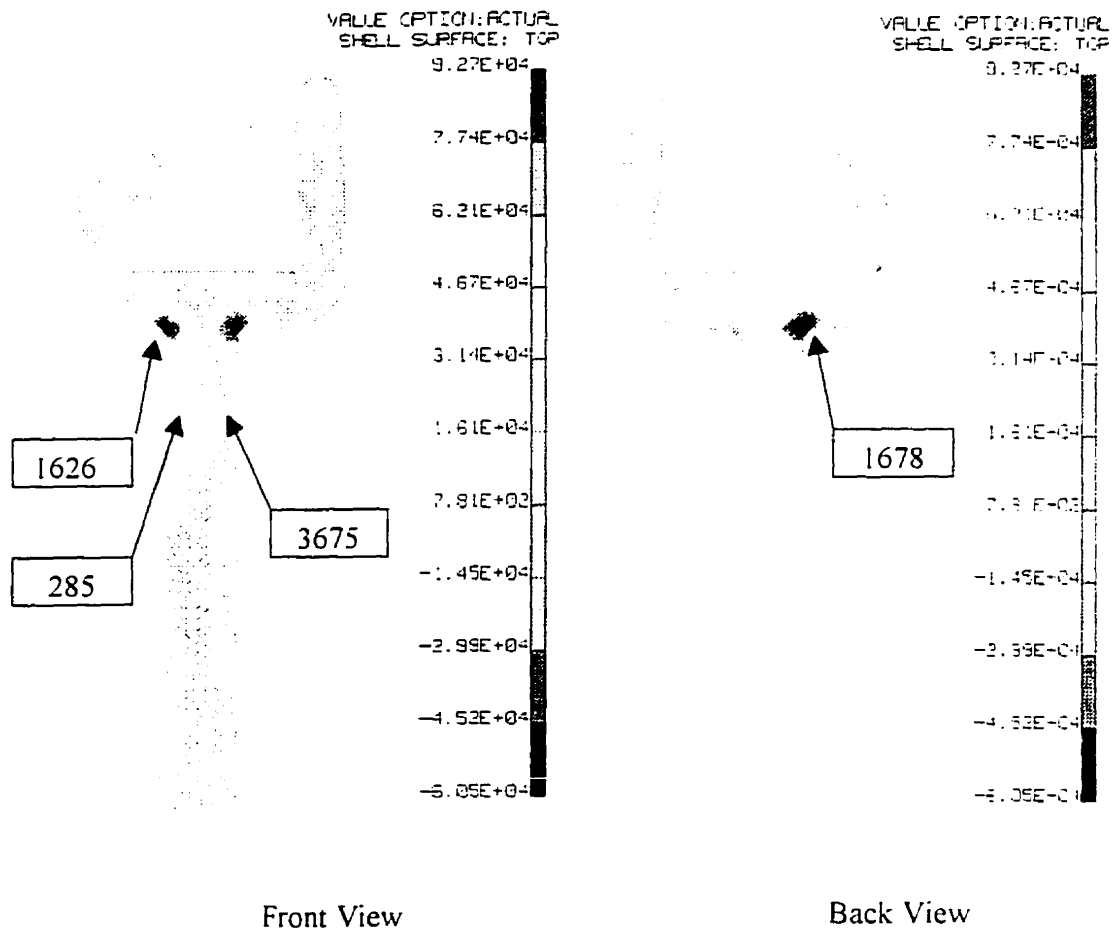*Direction:* -Y direction of the default coordinate system in FEM model. This direction is perpendicular to the aerobar extension, and towards the ground.
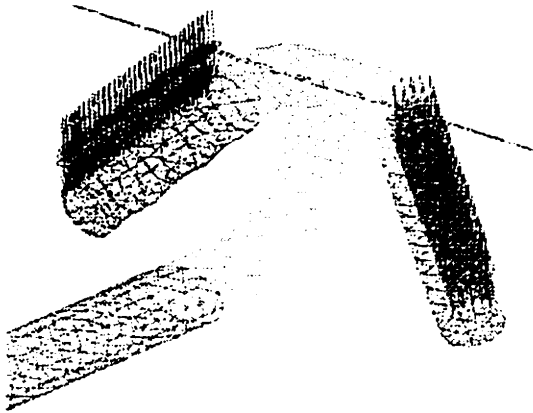
Figure 3.17 FEM Model for Vader, Downward Load

Stress Results:

The stress distribution contours for this case are shown in Figure 3.18, the numbers in the boxes are the node numbers of the maximum and minimum stress by using Maximum Principle Stress criteria.

The table that follows lists the maximum principle stress, maximum shear stress and the Von Mises stress values for this load case, and the node numbers corresponding to these stress values are also listed.
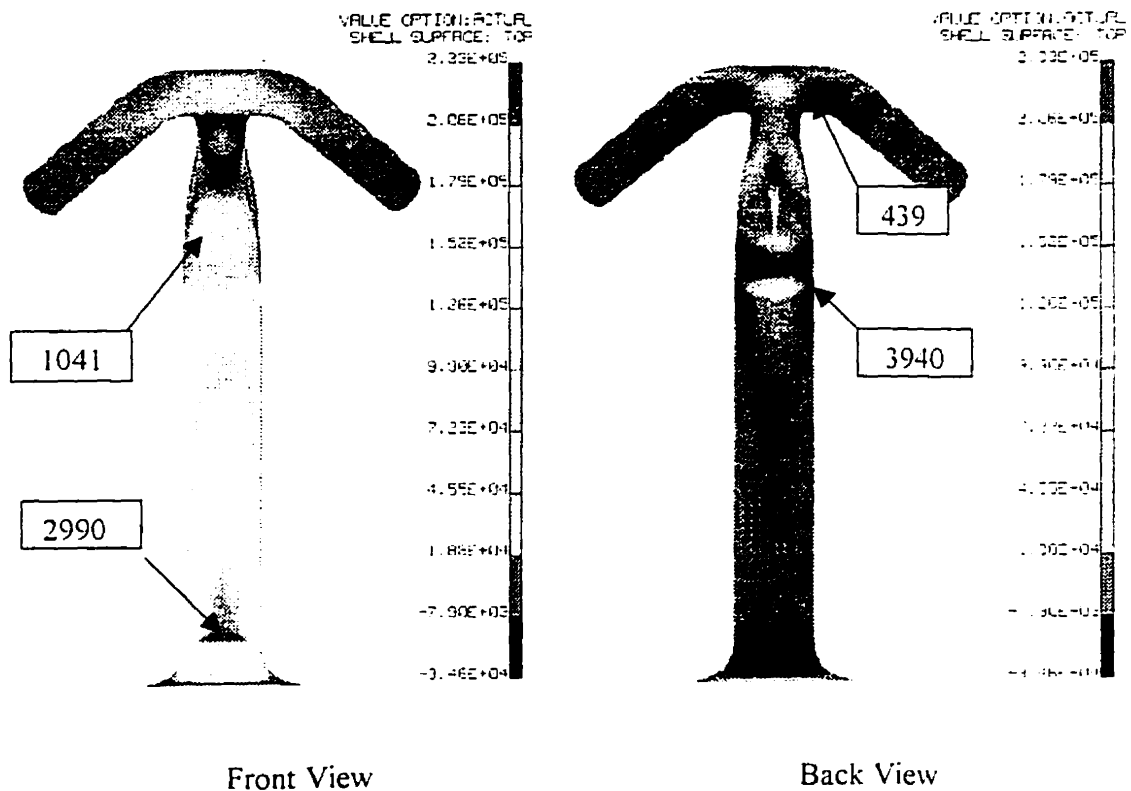
Figure 3.18 Stress Distribution for Vader, Downward Load

		Max. Prin.	Max. Shear	Von Mises
Aerobar bar-end	Node	1041	1066	1066
	σmax	8.313e4	6.276e4	1.192e5
	Node	439	2254	2254
	σmin	-3.558e4	36.51	68.35
Handle-bar	Node	2990	2990	2990
	σmax	2.326e5	1.163e5	2.236e5
	Node	3940	2560	2560
	σmin	-2.606e4	1.47e2	2.772e2

Table 3.18 Stress Result for Vader, Downward Load

The following table shows the maximum and minimum node displacements for this load case. The maximum displacement magnitude is also listed; "M.D.M." in the table stands for this value.

	Disp-X (mm)	Disp-Y (mm)	Disp-Z (mm)	Disp-RX (rad)	Disp-RY (rad)	Disp-RZ (rad)	M.D.M. (mm)
Node	728	2783	838	2886	1072	2498	
Maximum	4.29	2.019E-02	16.48	9.545e-04	8.543e-02	0.148	
Node	2223	337	2553	1081	1085	14	22.3
Minimum	-4.276	-19.29	-1.318e-2	-0.2811	-8.59e-2	-0.1451	

Table 3.19 Maximum and Minimum Node Displacements for Vader, Downward Load

Discussion:

From the FEA results, for the aerobar bar-end, the maximum tensile stress appears to be near the interface area with the aerobar extension. The maximum compression stress appears to be in the area where the grips merge with the elliptical section. In the

back view, there are some higher tensile stress areas. This is because the two 50Kg loads create a moment, which is along the X direction in this area.

For the aerobar extension, the maximum tensile and compression stresses are near the clamped end, because the moment in this section is the highest. The reason for the sudden change of stress near the clamped area is the same as stated before. In the back view, there is a small tensile stress area; this is due to the shape change in geometry.

3.4.3.2 Load Case 2: Inward load

Load:

Total force: 100Kg, i.e. 980N on the front cylindrical surface, furthest away from the rider.

Direction: Z direction of the default coordinate system in FEM model. This direction is parallel to the ground and the aerobar extension, and opposite to the riding direction.
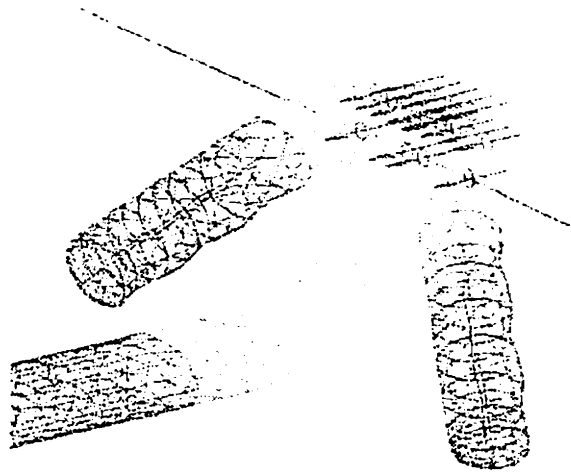

Figure 3.19 FEM Model for Vader, Inward Load

Stress Results:

The stress distribution contours for this case are shown in Figure 3.20, the numbers in the boxes are the node numbers of the maximum and minimum stress by using Maximum Principle Stress criteria.

The table that follows lists the maximum principle stress, maximum shear stress and the Von Mises stress values for this load case, and the node numbers corresponding to these stress values are also listed.

Front View   Back View
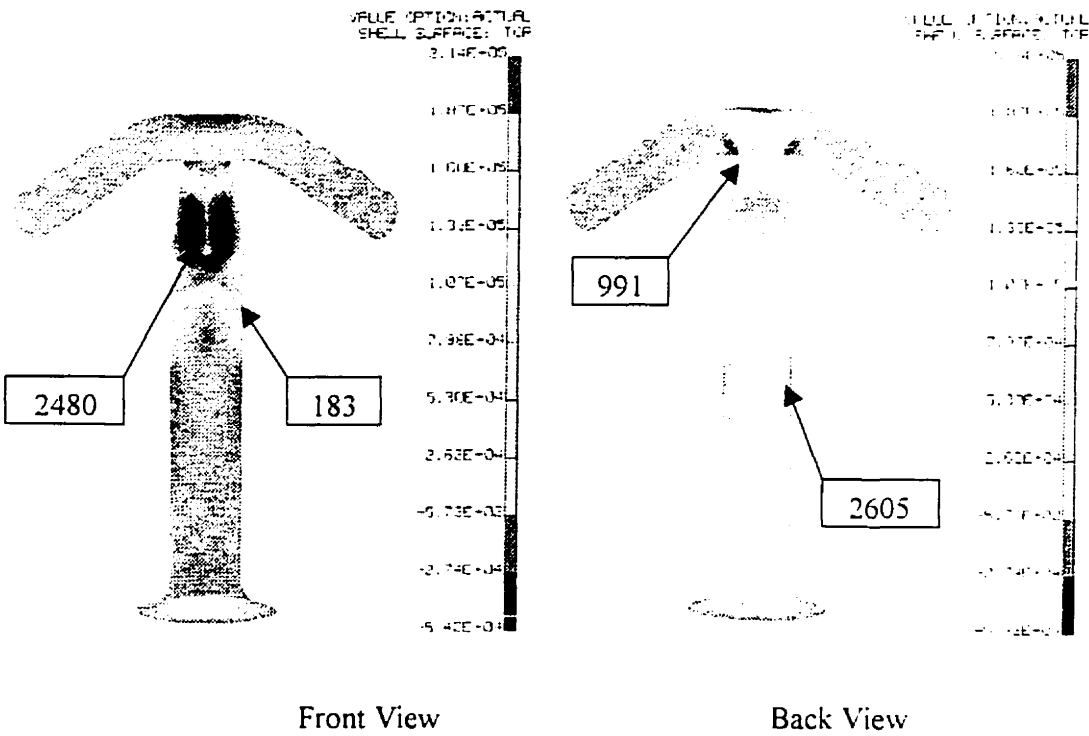
Figure 3.20 Stress Distribution for Vader, Inward Load

		Max. Prin.	Max. Shear	Von Mises
Aerobar bar-end	Node	991	2480	2480
	σmax	1.54e5	1.136e5	2.051e5
	Node	2480	889	889
	σmin	-5.553e4	6.887	11.94
Handle-bar	Node	183	193	193
	σmax	2.247e5	1.747e5	3.064e5
	Node	2605	2558	2558
	σmin	-1.469e4	30.6	55.02

Table 3.20 Stress Result for Vader, Inward Load

The following table shows the maximum and minimum node displacements for this load case. The maximum displacement magnitude is also listed; "M.D.M." in the table stands for this value.

	Disp-X (mm)	Disp-Y (mm)	Disp-Z (mm)	Disp-RX (rad)	Disp-RY (rad)	Disp-RZ (rad)	M.D.M. (mm)
Node	1098	1420	1073	1	1085	14	
Maximum	2.724	**43.19**	2.09	**0.8111**	0.3	0.4416	
Node	1059	895	47	177	1072	2498	**44.2**
Minimum	-2.74	-10.48	-18.16	-0.1635	-0.2991	-0.4515	

Table 3.21 Maximum and Minimum Node Displacements for Vader, Inward Load

Discussion:

From the FEA results, for the aerobar bar-end, the maximum tensile stress appears to be on the joint area of the elliptical section merging with the grips; the maximum compression stress is near the interface area.

For the aerobar extension, the maximum tensile and compression stresses are almost the same everywhere, because the force and moment stay constant through the whole area.

On the aerobar extension, there are two very small areas near the interface with the bar-end, in which the tensile stress is much higher than in other areas, and the maximum stress is located in these small areas. This is stress concentration due to the change of material and thickness. This stress can be ignored because it is caused by the finite element formulation, which cannot properly calculate stresses in regions of sudden stiffness change.

3.4.3.3 Load Case 3: Twist load

Load:

Total force: 50Kg X 2 on each model, i.e. 40.8333N on each surface of 24 surfaces.

Direction: ±Y direction of the default coordinate system in FEM model. This direction is perpendicular to the ground and the aerobar extension.
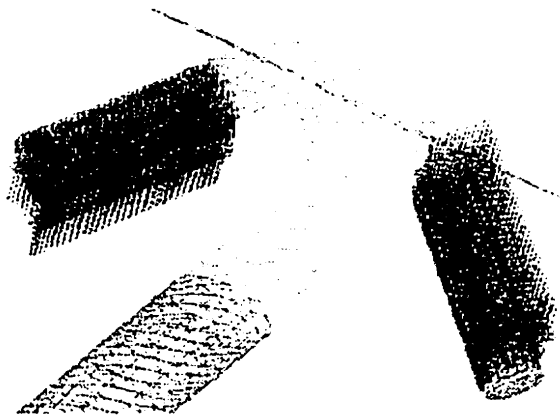

Figure 3.21 FEM Model for Vader, Twist Load

Stress Results:

The stress distribution contours for this case are shown in Figure 3.22, the numbers in the boxes are the node numbers of the maximum and minimum stress by using Maximum Principle Stress criteria.

The table that follows lists the maximum principle stress, maximum shear stress and the Von Mises stress values for this load case, and the node numbers corresponding to these stress values are also listed.

Front View   Back View
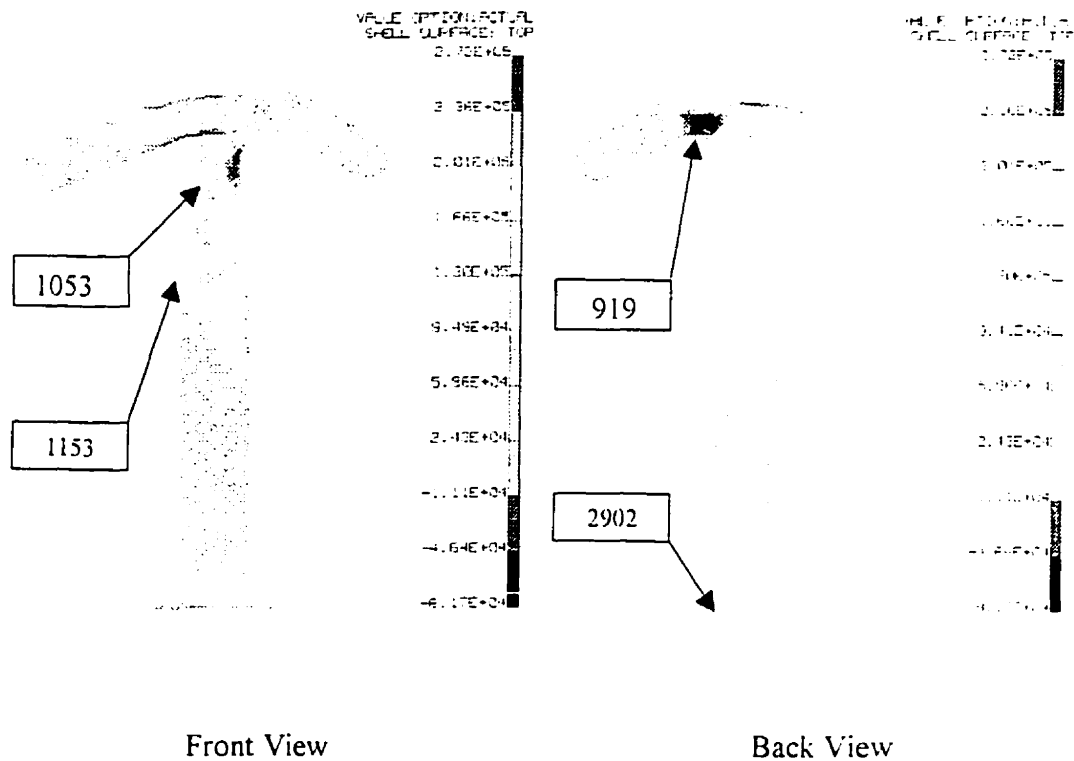
Figure 3.22 Stress Distribution for Vader, Twist Load

		Max. Prin.	Max. Shear	Von Mises
Aerobar bar-end	Node	1053	996	996
	σmax	2.717e5	1.453e5	2.895e5
	Node	919	824	824
	σmin	-8.367e4	18.43	35.81
Aerobar Extension	Node	1153	1153	1153
	σmax	1.571e5	1.332e5	2.319e5
	Node	2902	2560	2560
	σmin	-3.513e2	38.79	67.18

Table 3.22 Stress Result for Vader, Twist Load

The following table shows the maximum and minimum node displacements for this load case. The maximum displacement magnitude is also listed; "M.D.M." in the table stands for this value.

	Disp-X (mm)	Disp-Y (mm)	Disp-Z (mm)	Disp-RX (rad)	Disp-RY (rad)	Disp-RZ (rad)	M.D.M. (mm)
Node	1371	1298	2101	1063	12	2455	
Maximum	30.05	45.63	57.81	0.4158	9.348e-2	9.464e-2	
Node	2224	815	844	1093	1079	1022	76.7
Minimum	-23.92	-48	**-60.1**	-0.3611	**-0.661**	-0.5803	

Table 3.23 Maximum and Minimum Node Displacements for Vader, Twist Load

Discussion:

The area, in which the elliptical section merging with the grips is critical for Vader, this area has higher stresses than other parts for twist load case.

3.4.3.4 Summary of FEA Stress Results for Vader:

	Aerobar extension		Aerobar bar-end	
	σmax	σmin	σmax	σmin
Load Case 1	**2.326e5**	**-2.606e4**	8.313e4	-3.558e4
Load Case 2	2.247e5	-1.469e4	1.54e5	-5.553e4
Load Case 3	1.571e5	-3.513e2	**2.717e5**	**-8.367e4**

Table 3.24 Maximum Stress Summary of Vader

From the above table, we see that for aerobar bar-end, the downward load case is the worst case, maximum stresses for both tensile and compression are the biggest among the three load cases. Maximum stress due to inward load is also high. The abilities to withstand the impact load and the rider's body weight are critical for Vader bar. Like Claw bar, increasing the radius of the round corner will also improve resistance to impact.

For the aerobar extension, the twist load is the worst case, maximum stress for both tensile and compression is the biggest among the three load cases.

3.5 Discussions and Conclusion

For convenience, Table 3.25 summarizes the maximum tensile and compression stresses for the three aerobars, as follows:

		Downward Load	Inward Load	Twist Load
Mantis	Bar-end	σmax = 67.5	σmax = 92.54	σmax = 62.51
		σmin = -24.92	σmin = **-100.5**	σmin = -34.9
	Extension	σmax = **251.1**	σmax = 155.6	σmax = 29.35
		σmin = -27.52	σmin = -14.25	σmin = -0.2213
Claw	Bar-end	σmax = **120.06**	σmax = 116.6	σmax = 94.37
		σmin = -58.78	σmin = -57.41	σmin = -62.37
	Extension	σmax = 230.7	σmax = 57.39	σmax = 55.31
		σmin = **-30.29**	σmin = -8.146	σmin = **-6.407**
Vader	Bar-end	σmax = 83.13	σmax = **154**	σmax = 271.7
		σmin = **-35.58**	σmin = -55.53	σmin = **-83.67**
	Extension	σmax = 232.6	σmax = **224.7**	σmax = 157.1
		σmin = -26.06	σmin = **-14.69**	σmin = -0.3513

Table 3.25 Maximum Stress Summary for the Three Aerobars

Compare the tensile and compression strength of LTM25/CF0511 (see Table 2.1) with the maximum and minimum stresses in the aerobar extension, we see that for a 2mm thickness, the maximum and minimum stresses in all cases are less than the tensile and compression strength of the material, so the aerobar extension will not fail under any of the load cases, safety factor are all greater than 2.

Also from the FEA result, we conclude that the design of Mantis is the best in the sense that it behaves the best among the three designs under all the three loads. Vader is better than Claw in downward load, while Claw is better than Vader in inward load. For twist load, they are similar in the sense that the maximum tensile stress in Vader is bigger than that in Claw, while the maximum compression stress in Claw is bigger than that in Vader.

Using the Maximum Principle Stress Criteria, and comparing the stress values in Table 3.25 with the strength values in Table 2.1 and Table 2.2, Table 3.26 will be obtained. In this table, "S" stands for safe, "F" stands for fail.

		Downward	Inward	Twist
Mantis	Bar-end	F	F	S
		S	F	S
	Extension	S	S	S
		S	S	S
Claw	Bar-end	F	F	F
		S	S	S
	Extension	S	S	S
		S	S	S
Vader	Bar-end	F	F	F
		S	S	F
	Extension	S	S	S
		S	S	S

Table 3.26 Summary of Failure for the Aerobars

Efforts were also put on the optimization of the current design, like trying to change the radius of the round corners on Claw and Vader bars, but the FEA result shows that the improvement is very limited. This is because the changes that can be done are very limited if we keep most of the dimensions and shapes of the current design.

In order to find a proper plastic for the aerobar bar-ends, use the material property search in the Matweb homepage [29], which is a free materials information database with data on 23,856 materials including metals, plastics, ceramics, and composites.

Considering the FEA results and the above requirements, set the search range as "ABS polymer" and "Nylon", which are thermoplastics. Set the minimum compressive yield strength and minimum tensile yield strength as 10 MPa and 100 MPa, respectively. The search result shows that both ABS and Nylon have to be reinforced with glass or carbon fiber in order to satisfy the yield strength requirements. But the glass or carbon fiber reinforced ABS or Nylon cannot be cast or molded. This is the contradiction.

If the aerobar bar-ends are made using carbon fiber, the thickness might be less than 3mm and all of them will be safe under the loads. The disadvantage of using carbon

fiber is that the cost is too high, and the fabrication process is complicated compare with metal and/or plastic.

The tensile yield strength of aluminum alloy that can be cast is 120~295 MPa [1], which is much higher than that of plastic, if properly selected, the tensile yield strength can be bigger than the maximum tensile stress from the FEA results for aerobar bar-ends.

The density of aluminum alloy is around $2.7 g/cm^3$ [1]; this is higher than the density of ABS, which is around $1 g/cm^3$ [29], and the density of Nylon, which is around $1.27 g/cm^3$ [29]. But the volumes of the three aerobar bar-ends are not very big if the thickness is 3mm. For example, the Mantis will weight 60g if made with ABS and 3mm thickness, so if aluminum alloy is used as the material, the weight will only increase 102g, which is not too much for a bicycle.

The disadvantage of using aluminum alloy as an aerobar bar-end material is that the cost is higher than using plastic. Moreover, it is very hard to cast it using the facilities in the lab.

The material selection for the aerobar bar-ends will be a topic for future research work.

Chapter 4 Experimental Verification

4.1 Objective of Experimental work

Although FEA is a very good and effective analysis method, it is a theoretical, idealized model of a real structure. Furthermore, if the structural is complicated enough, I-Deas will sometimes yield erroneous result. For this reason, we cannot always rely on the FEM completely. Some experiments are important and necessary.

In this project, the Mantis is chosen for the tests because it is the easiest to build in the lab.

4.2 Introduction to Experiments

The laboratory work in this project is mainly focused on two aspects:

1) Find the appropriate method to build a hollowed aerobar bar-end prototypes with required thickness

2) Perform static load tests on the sample aerobar bar-ends

From the FEA results, we concluded that the aerobar extension will not fail under any of the given load cases, so the primary objective of this project is to focus on aerobar bar-end, for this reason, we tested only the aerobar bar-end.

4.3 Fabrication of Hollowed Aerobar Bar-ends

The prototypes were meant to simulate actual manufactured parts. However, an expensive injection molding process using ABS will be used to make the final production parts. The procedure used here is a way to produce a few prototypes at relatively low cost. Thus the fabrication procedure used is merely for prototypes and not for production. The procedure is described by first listing the fabrication materials, then the manufacturing process and finally, the finishing.

4.3.1 Fabrication Materials

Because this is a laboratory work, cost is a very important aspect. We have to use common and cheap material as much as possible. All the material used in this project are easier to find and cheap to buy.

RP-6430

In order to use the existing facility in the lab to fabricate the aerobar bar-end, we choose another material to replace the ABS. The mechanical properties of this material are similar to ABS.

The material used for fabricating the aerobar bar-end is RP-6430 [31]. RP-6430 is liquid at room temperature so it is easy to mix. It can be used in conventional casting, vacuum casting, pressure casting and meter mixing. The main properties of this material are listed below [31].

Mix Ratio	Mixed Viscosity	Gel Time	Maximum Cast Thickness	Minimum Demold Time
Resin to Hardener by Wt.	Cp@77°F (25°C) after 5 min.	Min.	in.	Hrs.@ 77°F(25°C)
100/50	200	20	0 5	24
Cured Density	Tensile Strength	Tear Strength	Elongation	Price (With hardener)
g/cm³	psi	ppi	%	CDNS
1.14	5900	425	13	196.19/gallon

Table 4.1 Properties of RP-6430

The problem that may be encountered for using RP-6430 is that foam may appear on the surface. In order to prevent this, the mixing container should be dry and nonporous; the mold should be dry and clean. An out-gassing procedure is used to ensure

proper mixing and removal of all foam and babbles. The RP-6430 is subjected to a vacuum pressure for about 5-10 minutes before being poured into the mold.

40% Sodium Silicate solutions [32]

This is used with fine sand to fabricate the core for the hollowed aerobar bar-end.

Sheet Wax [33]

A layer of 3mm thick wax is used to take the space for RP-6430 in the mold. The core is made in the mold filled with this wax.

Sand [34]

Dried all purposes fine sand with the 40% sodium silicate solution is used to make the core.

Mold Sealing Wax [35]

This is used to cover the mold surface, to separate the mold surface from the cast material, and to make the removal of the aerobar bar-end casting easy. The wax is otherwise known as a "mold release agent".

Carpenter's Glue [36]

This is used to cover the core surface, otherwise, the RP-6430 will penetrate into the sand core, and as a result, the core will not dissolve in water.

Besides the materials stated above, an electronic-weighting system, which is used to measure the RP-6430 and the hardener, is also required.

4.3.2 Fabrication Process
4.3.2.1 Make Half Cores

The core that is used to make the hollowed aerobar bar-end is a very important part of this project. There are three conditions that the core must satisfy.

1) The material of the core should not react chemically with the RP-6430

2) After casting the aerobar bar-end, the core must be taken out easily

3) The surface of the core should be fine enough to ensure that the inside surface of the aerobar bar-end is fine, to eliminate the internal defects in the aerobar bar-end.

After some investigation work, fine sand with sodium silicate solution was chosen to make the core. Sodium silicate cores can be dissolved in water again after they are dried.

In order to make a 3mm thick aerobar bar-end; a plate of 3mm wax is used to make the core. The process is the following.

1) Put the 3mm wax into the two half molds, press on it, and make sure that there has no clearance between the wax and the mold.

2) Remove the extra wax.

3) Pave a thin film of plastic on the wax, which separates the core and the wax, makes it easier to remove the core after it get dry.

4) Strain the sand by a fine strainer

5) Mix 10 portions of the sand with 1 portion of the sodium silicate solution by weight. Mix them thoroughly till all sand looks like wet.

6) Put the mixture into the two molds, press it and flatten the surface of mold interface.

7) Leave the mixture in the mold till it becomes solid completely, then we get two half cores.

The above procedure is shown by pictures follows:
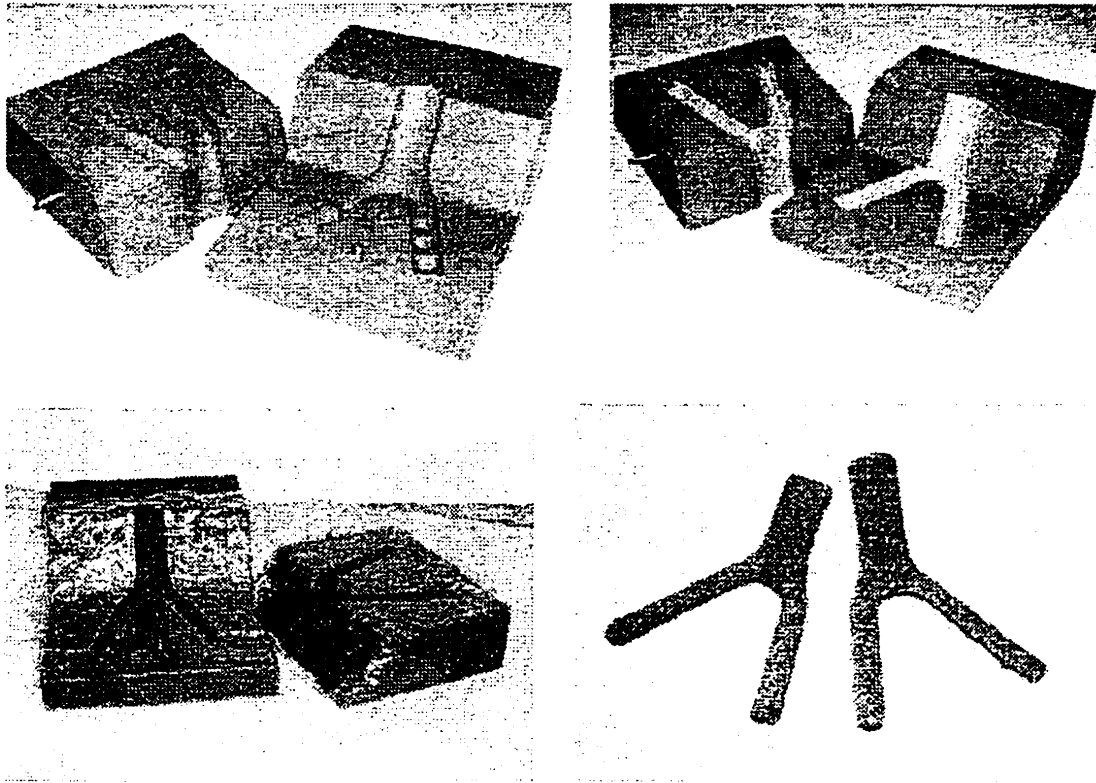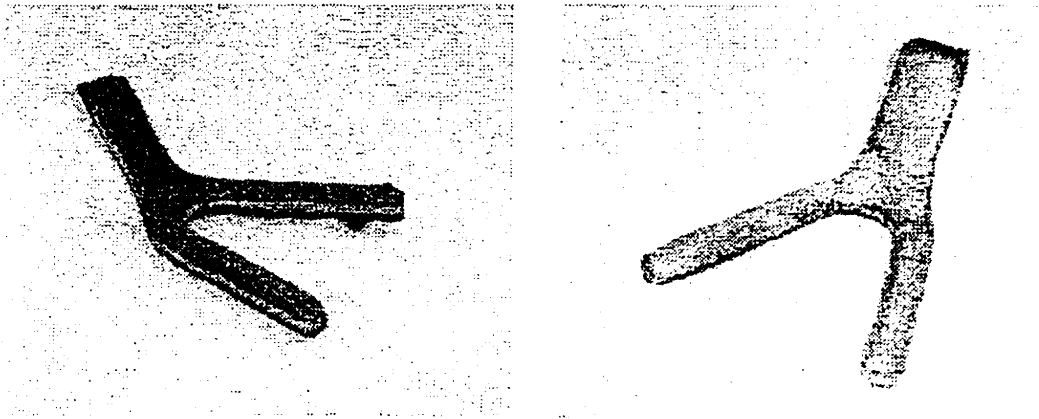
Figure 4.1 Make the half core

4.3.2.2 Make the Whole Core

After making the two half cores, and using carpenter's glue to stick them together, then a whole core is obtained. Use the carpenter's glue to cover the surface of the core, to prevent the RP-6430 from penetrating into the core which will make the core impossible to dissolve into water after making the aerobar bar-end. The process of this step is as follows:

1) Put the two half cores together in one half of the mold and seal the interface with the glue

2) Close the other half of the mold. Leave it for an hour until the glue dries. The purpose for this is to make sure that the two half cores glue together in the right position and still can be fitted into the mold.

3) Open the mold, take out the core

4) Paint a thin layer of the glue on the whole core. Make sure to paint it everywhere. Leave it in one half of the mold to air-dry it.

5) If there are any concave surfaces on the core, fill them with the glue. Make the surface of the core is as smooth as possible

6) After the glue dries, repeat the above procedure for two more times.

7) In order to hold the core in the right position in the mold, three small convex holds should be made. Stick three small pieces of 3mm wax on three different places of the core, best at the tip of the two grips and near the feeding head. The tips of the grips are not critical in bearing loading; the place near the feeding head will be cut off.

The pictures in Figure 4.2 show the result of the above process.

Figure 4.2 Completed Core

The important thing in this process lies on:

1) Use the carpenter's glue to compensate for flaw in the sand core; try to make the surface as flat as possible

2) When gluing the two half cores together, make sure that the core can still fit into the molds.

3) Make sure the core is painted with the carpenter's glue layer by layer and paint everywhere, do not leave the sand exposed anywhere.

4) Always leave the core in the mold; otherwise it is easier to get deflection due to the gravity even it is dry enough.

4.3.2.3 Make an Aerobar Bar-end

After finishing the making of the core, it is better to make the aerobar bar-end as soon as possible, to prevent the core from deflecting and deforming due to creep behavior.

1) Take out the wax layer from the mold.

2) Clean the mold use clear cloth

3) Wax the mold as follows [35]:

   - Apply the Ciba Wax with a soft lint-free towel
   - Use circular motion to work wax into surface
   - Cover approximately a 4-foot square area at a time
   - Allow wax to dry to a haze
   - Wipe with a clear towel until wax is glossy
   - Repeat above procedure two more times

4) Put the core into the mold, make sure it is in the right position, i.e. the clearance is the same everywhere

5) Close the mold, tight on it with a clamp.

6) Seal the crack of the interface with sealing wax [37]

7) Prepare the RP-6430 solution as follows:

   - Turn on the electronic-weighing system
   - Put a clean container on it and set the reading to zero
   - Pour 150g of RP-6430 into the container
   - Add 75g of the hardener into RP-6430 solution
   - Stir the solution to mix them completely
   - Eliminate the air bubbles in the mixture using a vacuum pump

8) Fill the mold with the solution very slowly to prevent creation of bubbles which will lead to air flaws in the aerobar bar-end

9) Leave the mold unmoved for 24 hours. The solution will become solid with a white color

10) Open the mold, take out the aerobar bar-end and put it into water, the core will become sand and sodium silicate solution once again. The glue will also dissolve in the water. Take out the sand; a hollowed aerobar bar-end is made.

The following pictures show the above procedure:
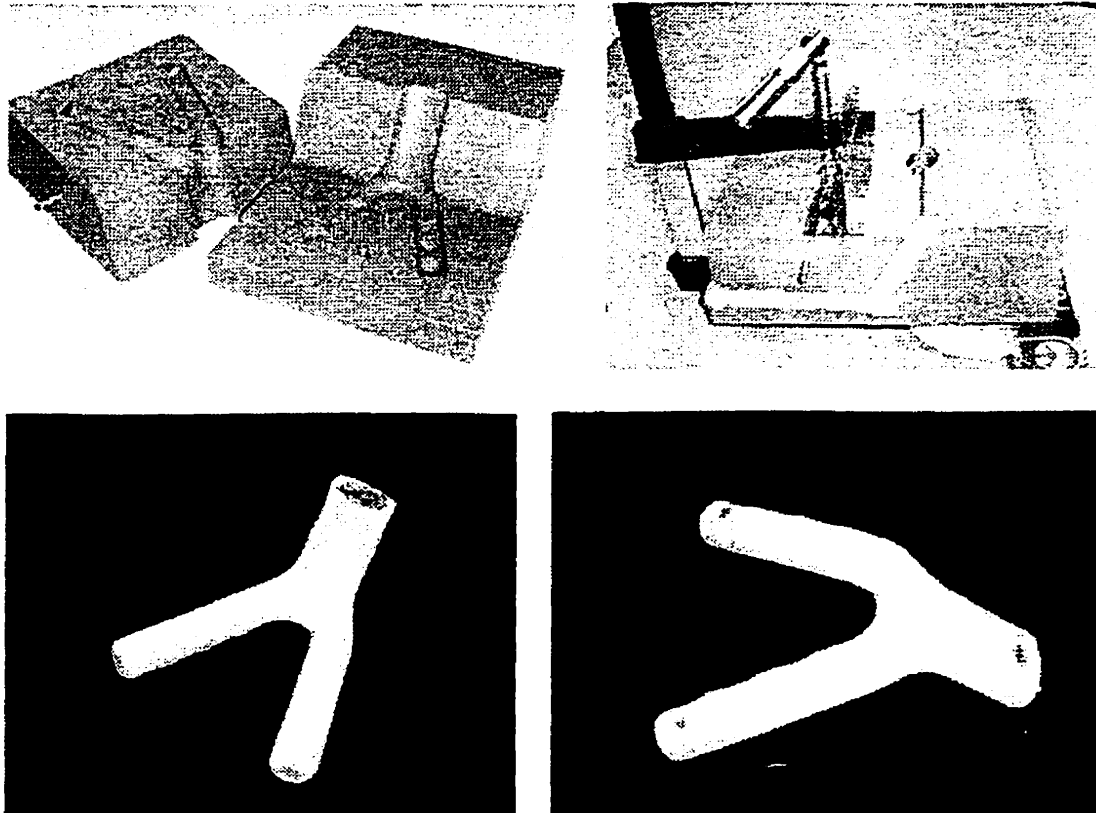
Figure 4.3 Making the Hollow Aerobar Bar-end

In the above process, the following points should be considered.

- RP-6430 and sodium silicate are all harmful to the human body, especially to the eyes. Protect hands and eyes properly.
- After the RP-6430 is mixed with the hardener, the time should be no longer than 15 minutes before it is poured into the mold, because the gel time for the RP-6430 is 20 minutes

- After finishing to pump the mixture, let the air go into the container very slowly. If the container is opened suddenly, air bubbles will be created in the mixture

- Tilt the mold when pouring the mixture, to let it flow down easily.

4.3.2.4 Attach the Plug into the Aerobar Bar-end

The aerobar bar-end has to be machined to a 2mm thickness at the interface with the aerobar extension. The thickness of the aluminum plug is 1mm, so that the total thickness is 3mm.

After finishing the machining, clean the plug and the aerobar bar-end with Acetone, and then use an Aluminum Etch Kit [38] to do the surface treatment on the plug according to the instructions. This will improve the bond force between aluminum and resin.

After the surface treatment on the plug, apply the resin evenly on the right surface of the plug using a brush, and then put the plug and the aerobar bar-end together as soon as possible. The resin will become solid in a few minutes, and then the plug and the aerobar bar-end are bonded together. The aerobar bar-end is ready to test. The following is the final picture of the bar-end with insert.
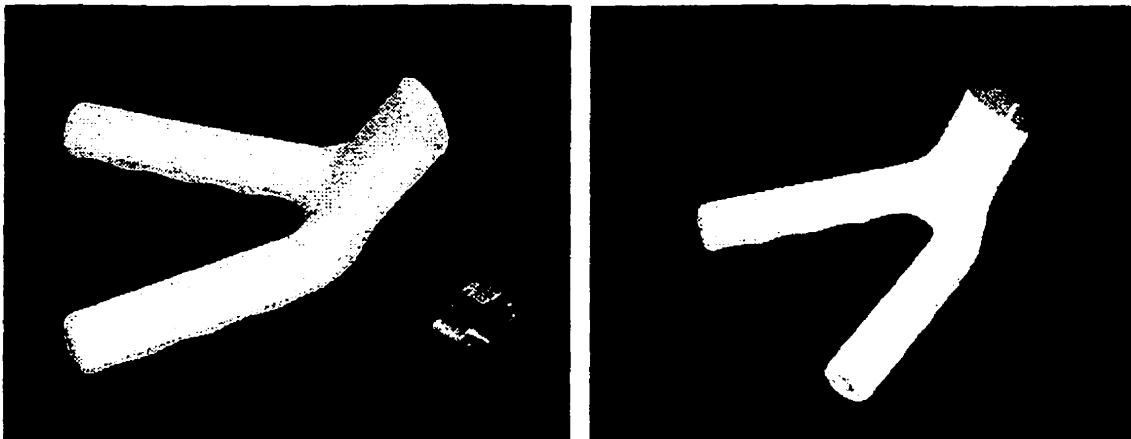
Figure 4.4 Completed Aerobar Bar-end with Insert

4.4 Design of the Test Attachments

In order to fix the three aerobar bar-ends onto the test device and put three different loads on them, some attachments are needed.
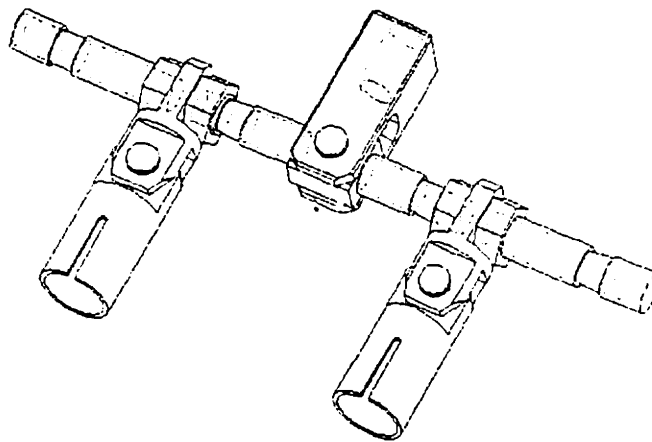
To fix the aerobar bar-end properly, the attachments should simulate the interface part of the aerobar extension, and at the same time, can be locked in the V-block of the testing device.

To put the distribution loads on the grips of the aerobar bar-end, the design uses caps and collars to simulate the load application.

The directions of the two grips of the aerobar bar-ends are different, and the three load cases also have different load application directions. The design uses joints to cover all of the loading possibilities.

The assembly of the test attachments is shown below. The material for all the parts is steel. The strength and stiffness of steel are strong enough to withstand the tests.

This test attachment can easily apply downward and inward loads on aerobar bar-end by screwing it on the piston cylinder of the test device. However, it is difficult to apply twist load by the existing test device.
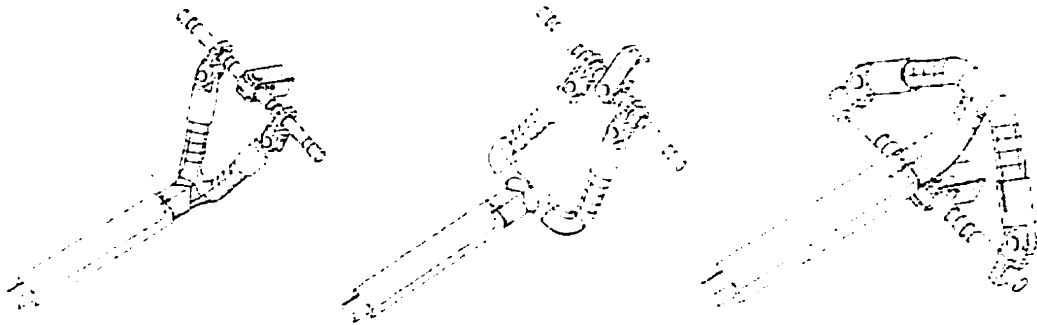

Figure 4.5 Aerobar Bar-end Test Attachment Assembly

Besides the parts shown above, a bar, which is used to replace the aerobar extension, and to fix the aerobar bar-end to the V-block on the test device, is also needed.

There are two screw holes on this part, which are the same as on the male plug. The material of this bar is also steel. The applications of the attachment to the three aerobar bar-ends are showing in Figure 4.6.

Figure 4.6 Application of the Attachment to the Aerobar Bar-ends

The drawings of this design are included in appendix A.

4.5 Static Tests on the Aerobar Bar-ends

The static tests are only performed on Mantis, and downward and inward loads are applied. The attachment for applying the twist load using the existing piston device is complicated and is thus not performed. The better choice is to supply input load with a device that can output a rotation torque, thus this current attachment will work.

### 4.5.1 Introduction to Bicycle Components Test Device [10]

The test device is composed of three parts: Mechanical, pneumatic and electronic.

The mechanical parts include: testing cable, fixtures that hold the piston and the piece being tested.

The pneumatic parts include: filter-lubricator-regulator, the proportional pressure controller, the reservoir, the solenoid valve and the piston.

The electronic elements include: computer, software, power supply, data acquisition cards, linear voltage transducer, back plane, connection boards and wiring

The following picture shows the test device:
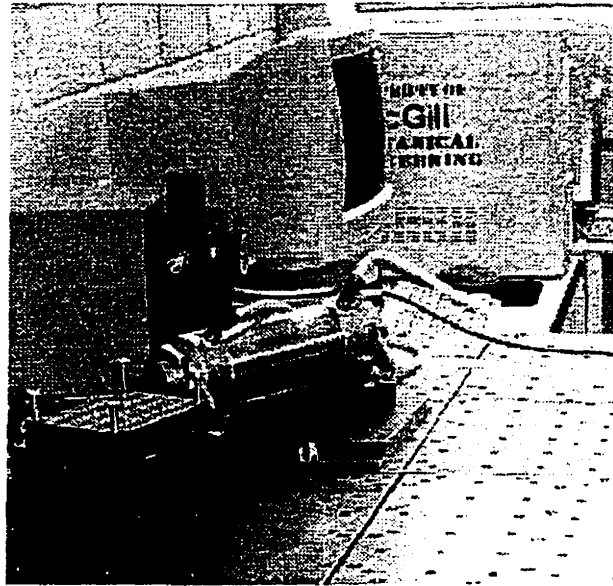
Figure 4.7 Bicycle Components Test Device

4.5.2 Test Under Static Downward Load

4.5.2.1 Failure Load calculation

From the FEA result, the maximum tensile stress for the Mantis under 100Kg downward load is 67.51 Mpa, while the tensile strength for RP-6430 is 5900 psi, which is 40 Mpa, therefore, the load F_f under which the bar start to fail will be

$$F_f = \frac{\sigma_y}{\sigma_{max}} \times F$$

$$= \frac{40}{67.51} \times 100$$

$$= 59.5(Kg)$$

This result shows that the Mantis bar will fail with 59.5 Kg downward load according to the FEA result.

4.5.2.2 Equivalent Load Calculation

In the FEM analysis, the distributed loads are put on the grips. While for the test attachment, the point where the load acts is away from the grips. For this reason, an equivalent load should be calculated for the test. The "equivalent load" here means that the load affects at the interface with the aerobar extension is the same in the test as in the analysis. The following picture shows the relationship between the actual load and the distributed load. For simplicity, replace the distributed loads with concentrated loads, which act at the middle of the distributed loads' action area.
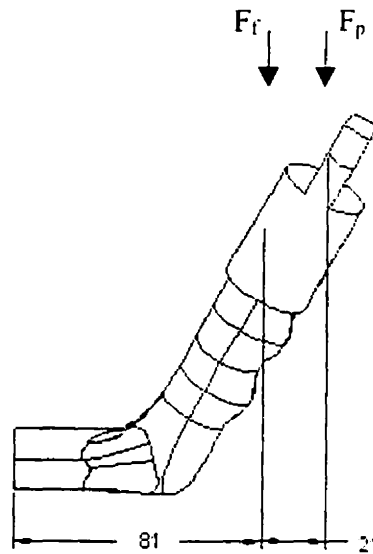
Figure 4.8 Mantis with Caps

The actual load F_p from the piston is calculated below.

$$F_p = \frac{d_1}{d_1 + d_2} \times F_f$$

$$= \frac{81}{(81 + 21)} \times 59.5$$

$$= 47(Kg)$$

$$= 461(N)$$

This result helps in setting the load range for the test.

4.5.2.3 Test Setup

Set up the test device as shown in the following steps. There are three aspects that are critical in these steps.

1) Rotate the steel bar in the V-block; make sure that the symmetric plane of the Mantis bar is horizontal. Otherwise, the load will not be a completely downward load.

2) Use shims if necessary, to make the symmetric plane of the Mantis bar and the centerline of the piston at the same level.

3) Adjust the relative position between the piston and the V-block, set the angle between the centerlines of the piston and the V-block at 90°, to simulate the situation where the downward load is perpendicular to the aerobar extension.
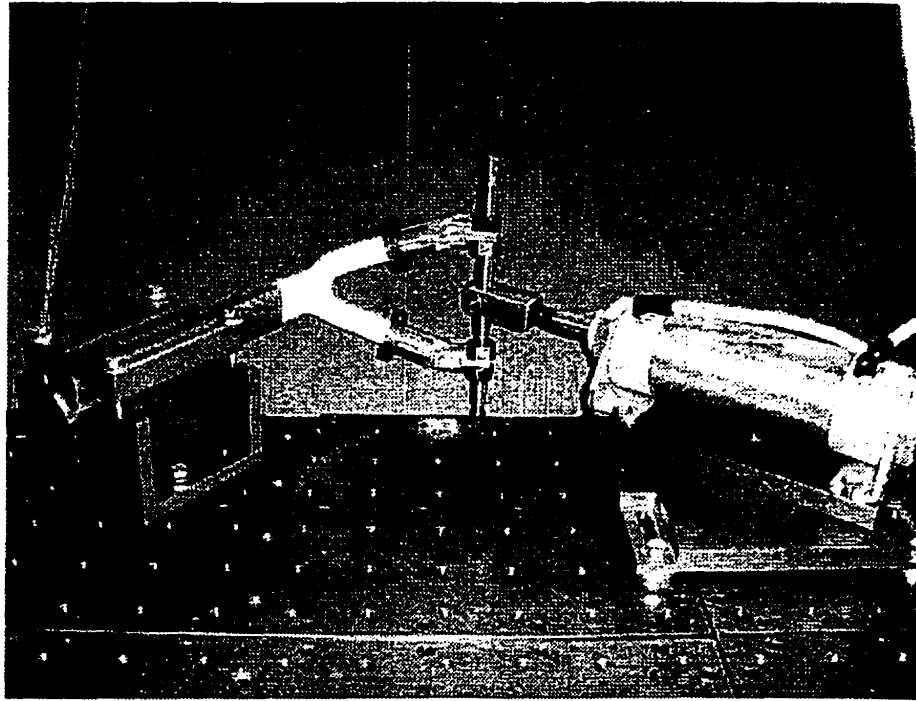
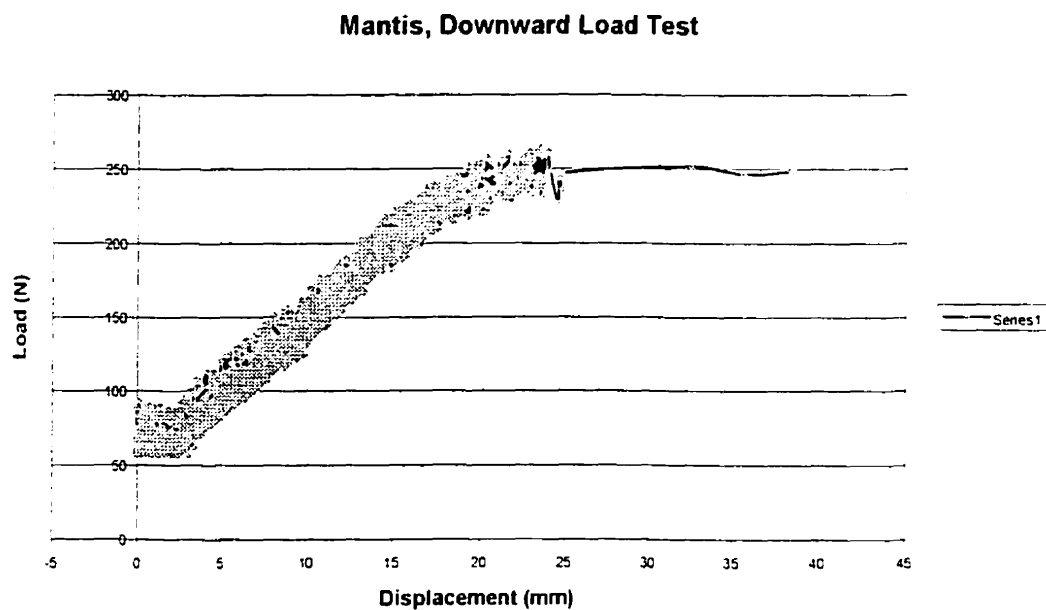**Figure 4.9 Mantis Downward load Test Set Up**

4.5.2.4 Test Procedure

After finishing the test setup, do the test follow the procedure outlined below:

1) Turn on the computer first, and then turn on the power of the test device.

2) Connect the two pressure air lines from the piston to the controller, making sure the panel is correct, i.e. inlet 1 and 2 from the piston should connect to the outlet 1 and 2 on the controller, respectively.

3) Start the test software, enter the " Calibration and Piston Limits " menu, and set the inward and outward displacement limits. Then enter the "Ramp Load" menu, set the "Peak Force" to a little larger than the equivalent load (in this case set it to 500N). Set "Duration of the Ramp" to 2 minutes. This means that the load will reach 500N in 2 minutes.

4) Create a path and file name for saving the data.

5) Click the "Start" button to begin the test. The displacement and the force data will be saved in the given file. The load will stop automatically after the Mantis fails.

6) When the test is finished, turn off the power of the test device first, then shut down the computer.

4.5.2.5 Test Result

When the load reached 250N, the Mantis broke in the bonding area, with the load and displacement curve is shown below. Figure 4.11 shows the failure detail for this test.

Mantis, Downward Load Test

Figure 4.10 Mantis Downward Load Test Result

Figure 4.11 Mantis Downward Load Test Failure Detail

4.5.2.6 Discussion and Conclusion

The failure occurs when the load reaches 250N and the location of the failure is at the bond between ABS aerobar bar-end and the aluminum insert. When the load is 250N, the moment at the bond is

$$M = 250 \times (81+21)$$
$$= 2.55 \times 10^4 \text{ (N.mm)}$$

The Maximum displacement is 38.4mm, which is bigger than analytical result, i.e. 23.8mm. This is reasonable because there are some clearances in the test attachment; this makes the displacement recorded bigger.

On the load-displacement curve, there are a total of 3505 points, among which there are many "noise points". However, even with these "noise" points, the linear relationship between the force and the displacement still can be seen, and the stiffness of the Mantis is about 10N/mm.

The displacement starts to occur when the load reaches about 75N, because at the beginning of the test, there is some clearance in the test attachment.

Failure occurs in the bonding region rather on the aerobar itself. This result shows that the bonding method or the material used for the insert needs to be improved.

74

4.5.3 Test Under Static Inward Load

4.5.3.1 Failure Load calculation

From the FEA result, the maximum tensile stress for the Mantis under 100Kg inward load is 92.53Mpa, while the tensile strength for RP-6430 is 40 Mpa, therefore, the load F_f under which the bar should start to fail will be

$$F_f = \frac{\sigma_y}{\sigma_{max}} \times F$$

$$= \frac{40}{92.53} \times 100$$

$$= 43(Kg)$$

This result shows that the Mantis bar will fail with 43 Kg of inward load according to the FEA result.

4.5.3.2 Equivalent Load Calculation

For the same reason as stated in section 4.5.2.2, the actual load F_p from the piston must be calculated as shown below:
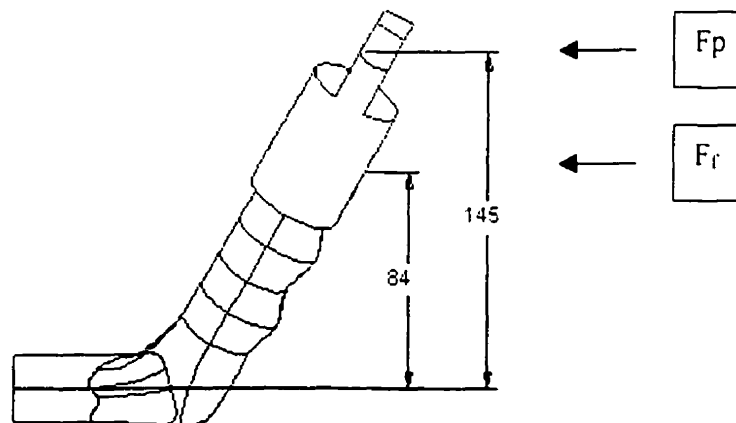
Figure 4.12 Mantis with Caps

$$F_p = \frac{h_1}{h_2} \times F_f$$
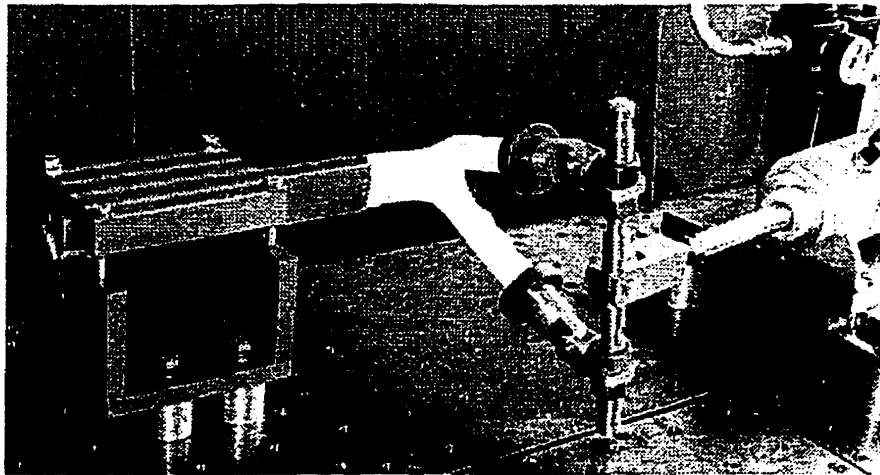
$$= \frac{84}{145} \times 43$$

$$= 24.9(Kg)$$

$$= 244(N)$$

The maximum load range for the piston in the test should be set according to this result.
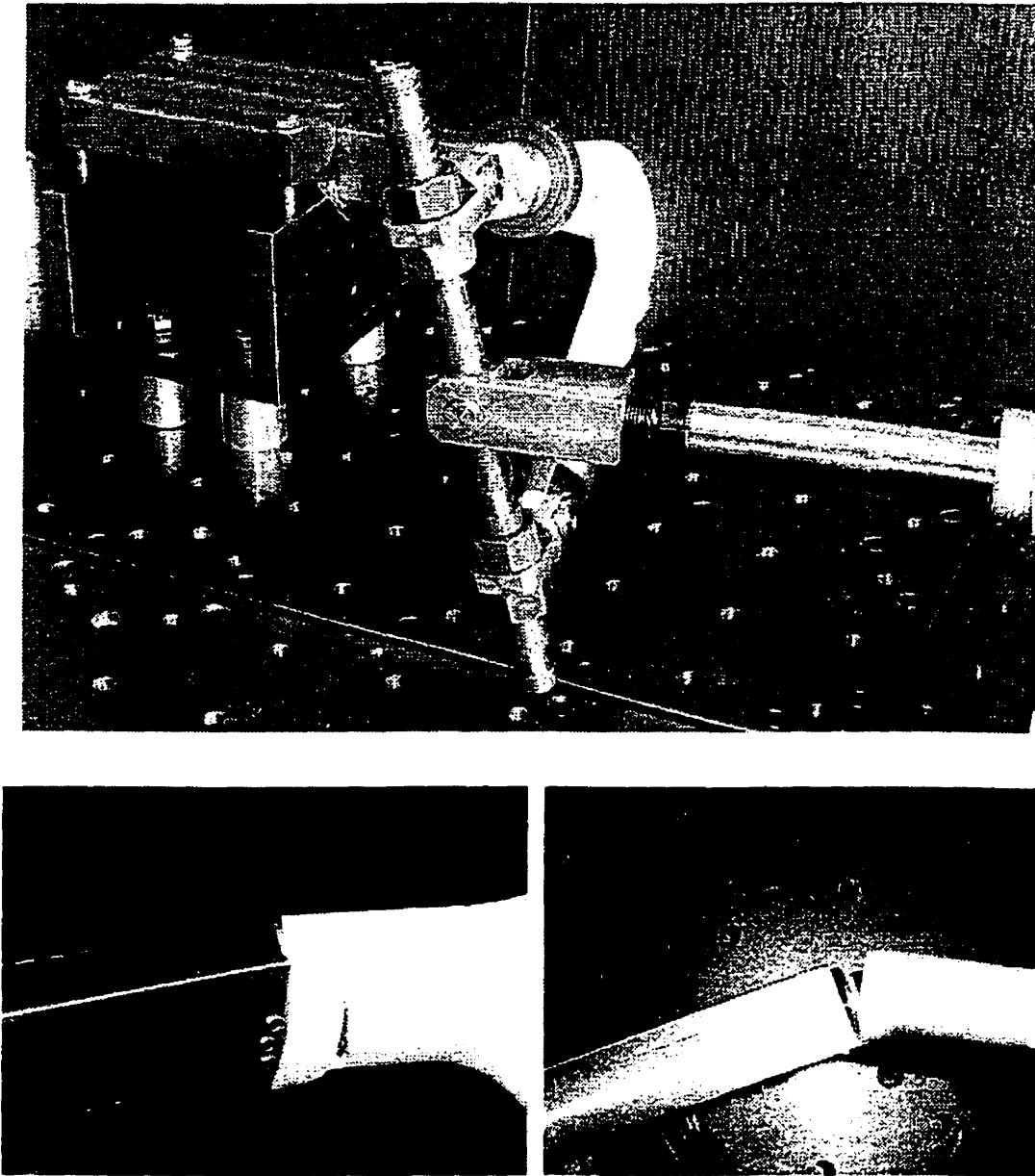
4.5.3.3 Test Setup

Set up the test device as shown below:
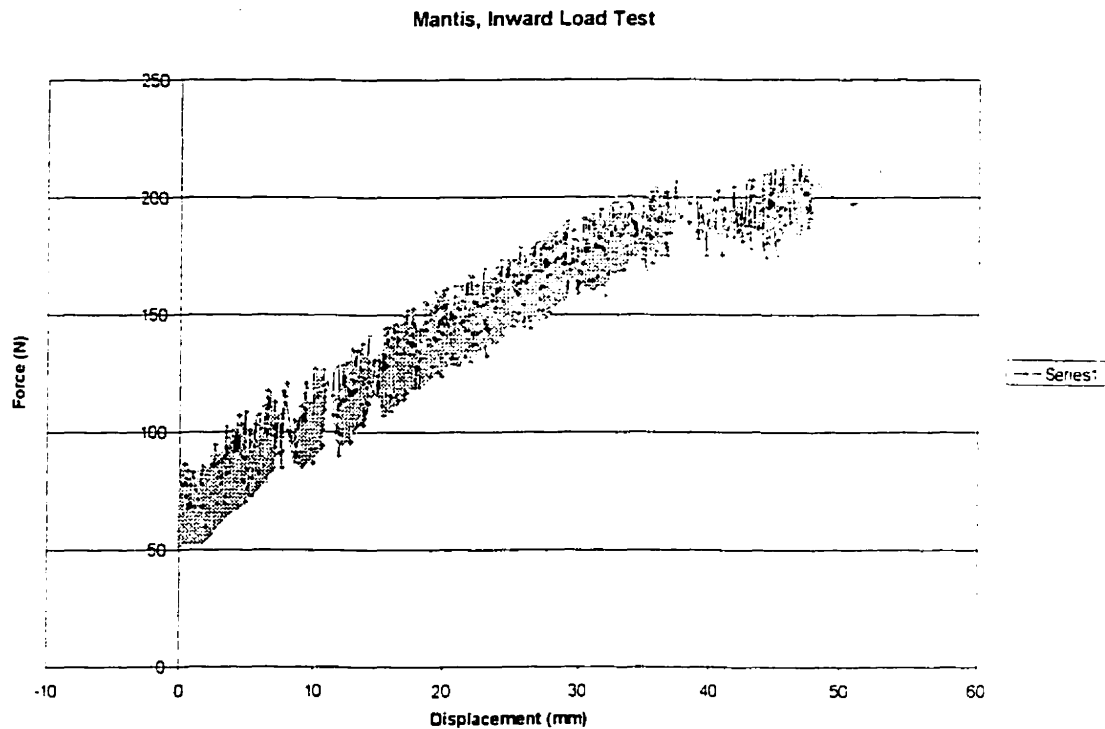

Figure 4.13 Mantis Inward Load Test Setup

4.5.3.4 Test Result

The Mantis broke when the inward load reaches 200N. The following figures show the detail of the test.

Figure 4.14   Failure Detail in Inward Test

The load and displacement relation in the inward test is shown below:

Mantis, Inward Load Test

Figure 4.15 Displacement-Load Curve in Inward Test

4.5.3.5 Discussion and Conclusion

The failure occurs when the load reaches 200N. Again, the bond between the aerobar bar-end and the insert fails.

The displacement starts when the load exceeds 50N, the maximum displacement is 52.644 mm, and this is also bigger than the analytical result, 33.4mm for the same reason stated in the downward test.

When the load is 200N, the moment at the bond is

$$M = 200 \times 145$$
$$= 2.9 \times 10^4 \text{ (N.mm)}$$

This moment causes the failure of the Mantis.

4.6 Discussions and Conclusion from the Tests

4.6.1 Problems Encountered and Their solutions

Totally, two downward load tests were performed on the Mantis. The first attempt did not give the maximum failure load due to some problems.

In the first test, in order to keep the thickness of the bonding area between the Mantis and the insert 3mm, the Mantis was machined to 1mm thick in the bonding area as designed in the previous project. Thus the thickness of the aluminum insert is 2mm. The first test shows that the 1mm thick for Mantis is far too weak, so starting from the second test, the thickness was changed to 2mm for the Mantis, and 1mm for the insert. The subsequent tests show that this is a reasonable improvement.

Again from the first test, the failure mode shows that the resin bonding between the Mantis and the insert is not as strong as it should be. The possible main reason for this is that the aluminum insert was not cleaned using Aluminum Etching Kit [30]. In the second test, the insert was cleaned using Acetone first, and then the bonding surface was etched using Aluminum Etching Kit. The failure mode shows that in this way, the bonding is improved significantly.

In the second test, the bonding area did not fail early due to the etch treatment on the insert. Another problem (at higher load) is that the Mantis with the insert loosens from the holding device. The reason for this problem is that there is about 1.5mm clearance between the aerobar extension replacement and the male insert on the Mantis. And the aluminum insert is too "soft" to use setscrews. Two small steel shims are used to solve this problem.

4.6.2 Conclusion from the Test

In the downward load test, the failure is in the bonding rather than in the RP-6430, and the load is only a little more than a half of the Mantis failure load. In the inward load test, the failure supposes to occur at the bottom of the grips, but in the test, the failure also occurs in bond area, and the failure loads in both cases are similar (in the downward load test, it is 250N, in the inward load test, it is 200N). These show that the resin bonding method between the RP-6430 and the aluminum is not as good as used

between two composite materials. The attachment method for the aerobar bar-end fixing to the aerobar extension will be a topic in the future research.

Chapter 5 Discussion and Conclusion

According to the Finite Element Analysis results, the aerobar extension will not fail under any of the load cases, safety factor are all greater than 2.

Also the FEA results show that the design of Mantis is the best among the three designs under all the three loads, because, generally speaking, the maximum stress values for Mantis are smaller than the Claw and the Vader. The radius of the corner on the Claw and the Vader need to be improved.

The Vader is better than the Claw in downward load, while the Claw is better than the Vader in inward load, but none of them will survive due to the high tensile stress. For twist load application, the Vader is the worst; both its maximum tensile and compression stresses are larger than the yield strength. While for the inward load application, the Mantis is the worst for the same reason.

The maximum compression stresses of the three bars are all smaller than the yield strength in downward load case.

The conclusion that can be drawn from the tests is that the resin bonding between the RP-6430 and the aluminum is not strong enough for the assumed load applications. A new attachment method for the aerobar bar-end fixing to the aerobar extension has to be founded.

Chapter 6 Significant Findings

The significant findings from this project are the following:

- By using Maximum Principle Stress criteria, the maximum tensile and compression stresses for the three aerobars in the three load cases are obtained;

- The designs of aerobar bar-ends need to be optimized, the three loads need to be re-considered;

- The 2mm thick carbon fiber aerobar extension will not fail in any of the load cases;

- The laboratory fabrication method for the hollow aerobar bar-ends was verified;

- The bounding method between the aerobar extension and the aerobar bar-ends needs to be improved.

Chapter 7 Suggestion to Further research work

From the FEA and the experimental results, further research work needed to be done on the aerobar.

First, the attachment method between the aerobar bar-ends and the extension needs to be modified. Tests show that the bonding between the aluminum insert and the plastic aerobar bar-end is not as strong as expected. Further study on the bonding or finding a new connection method is necessary.

From Table 3.26 in Chapter 3, we see that the ABS aerobar bar-end will not survive in any of the loads. Either modifies the loads (which are possibly too conservative) or re-select the material.

For the Claw and the Vader, design optimization is needed, to increase the curvature radius of the corners in order to reduce some stress concentration problems.

Study the fabrication and test method for industrial production can also be further research topic.
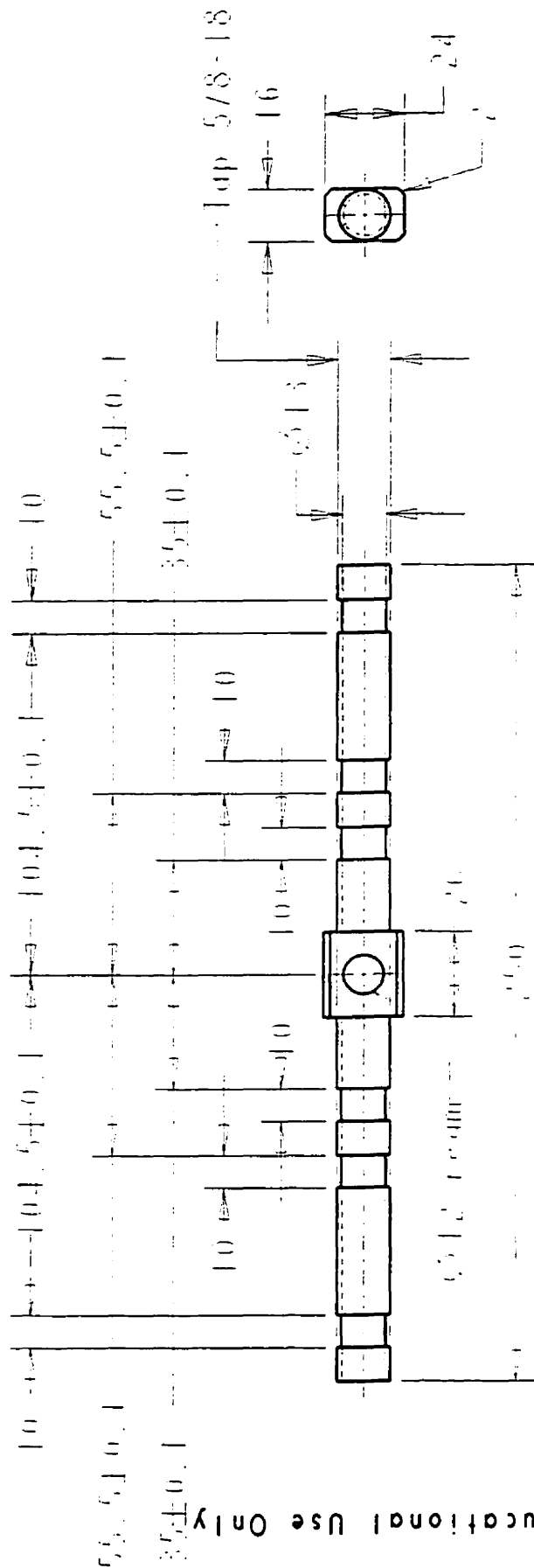
Reference

1. Harold A. Rothbart, *"Mechanical Design Handbook"*, McGraw-Hill, 1996

2. Zafer Gurdal, Raphael T. Haftka, Prabhat Hajela, *"Design and Optimization of Laminated Composite Materials"*, 1999

3. T.Nonweiler, *"Air Resistance of Racing Cyclists"*, report 106, 1956

4. C. R. Kyle, V. J. Caizzo, and P. Palombo, *"Predicting human-powered-vehicle performance using ergometry and aerodynamics-drag measurements"*, Proceedings of IMFA Conference, 1978

5. C. R. Kyle, *"The aerodynamics of man-powered land vehicles"*, Third National Seminar on Planning, Design and Implementation of Bicycle and Pedestrian Facilities, 1974

6. C. R. Kyle and W.E. Edelman, *"Man-powered vehicle design criteria"*, Third International Conference on Vehicle-System Dynamics, 1974

7. F. R. Whitt, *"Is streamlining worthwhile?"*, Bicycling, July 1972

8. C. R. Kyle, *"How Accessories Affect Bicycle Speed"*, engineering report, California State University, 1975

9. M.J. Turner, R.W. Clough, H.C. Martin and L.J. Topp: *Stiffness and deflection analysis of complex structures*, Journal of Aeronautical Sciences, 23, 805-824 (1956).

10. Brock A. Leong, *"A Testing Device For Bicycle Components"*, Project Report, 2000

11. Frank Rowland Whitt and David Gordon Wilson, *"Bicycling Science"*, The MIT Press, 1990

12. R. A. C. Fosberry, *"Research on the aerodynamics of road vehicles"*, New Scientist 6, August, 1959

13. http://graphics.stanford.edu/~lucasp/bike-aero.html

14. C.R. Kyle, *"Reduction of Wind Resistance and Power output of Racing Cyclists and Runners Traveling in Groups"*, Ergonomics 22:387-397, 1979

15. C.R. Kyle, *"Fast Fashion: the Aerodynamics of Bicycle Clothing"*, Bicycling 26(5): 118-125, 1985

16. C.R. Kyle, *"The Effect of Crosswinds upon Time Trials"*, Cycling Science, September and December, 1991

17. C.R. Kyle, *"The aerodynamics of Handlebars & Helmets"*, Cycling Science, December, 1989

18. http://www.syntace.com/

19. http://www.profile-design.com/

20. http://www.visiontechusa.com/

21. http://www.cinelli.it/english/

22. http://www.itm.it

23. http://www.cbike.com/

24. http://www.bicyclegear.com/

25. http://www.roadbikereview.com/

26. Ben Deeley, et al. *"The design and production of three prototype Aerobars for a Carbon Fiber Racing Bicycle"*, Project Report, McGill University, 2000

27. Lessard, L., *Course Notes: Mechanics of Composite Materials, Department of Mechanical Engineering*, McGill University, 1998

28. Charles A. Harper, *"Handbook of Plastics, Elastomers and Composites"*, McGraw-Hill, 1996

29. http://www.matweb.com

30. Singiresu S. Rao, *"The Finite Element Method in Engineering"*, Butterworth-Heinemann, 1999

31. Ciba Specialty Chemicals Corporation, USA, Product Data

32. PTI Process Chemicals, P.O. Box 148, CARY, IL

33. Freeman®, No. 165 Regular Sheet wax, adhesive-Back

34. SAKRETE®, KING Packaged Materials Company

35. Ciba Specialty Chemicals Corporation, Ciba Wax application instructions

36. Mastercraft®, Mastercraft Canada

37. Freeman®, sealing wax

38. West System®, 860 Aluminum Etch Kit, Gougeon Brothers, Inc. Bay City, MI, USA

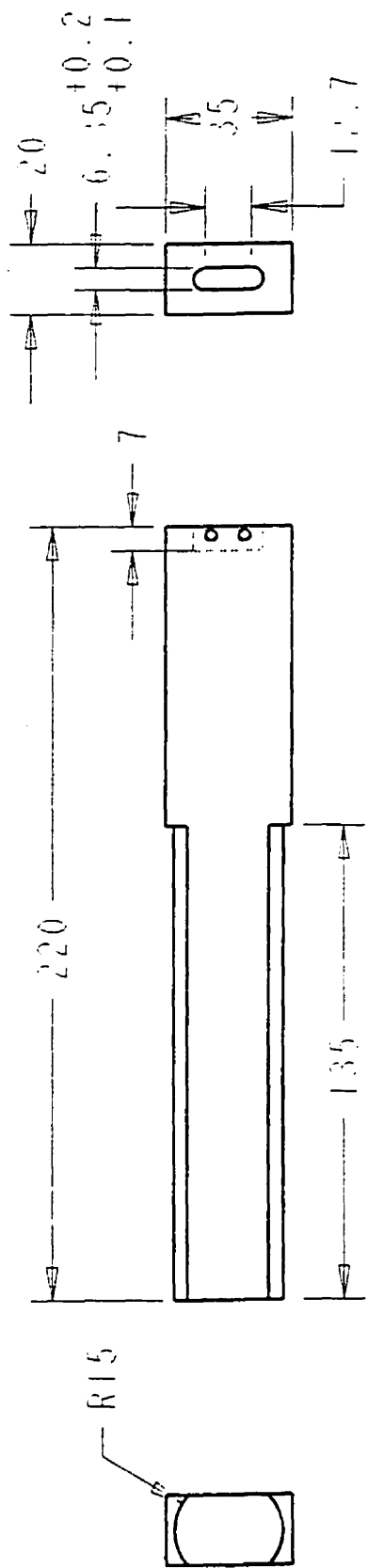**Appendix A**

DRAWINGS FOR AEROBAR BAR-END TEST ATTACHMENT

Tap 5/8-18

16

24

BEAM_REPLACE

PART NAME

DESCRIPTION

DRAWN BY

MATERIAL

QUANTITY

PART #

ALL DIMENSIONS IN mm

220

135

220

7

R15

20

6.5 +0.2
+0.1

35

1.7

For Educational Use Only

$10^{0}_{-0.1}$

38

25

$35°$

7

3

$\emptyset 12$ ream

$15^{+0.1}_{0}$

25

25

65

$\emptyset 25$

$\emptyset 18.6$

CAP

PART NAME

CONDITION

QUANTITY

PART #

DRAWN BY

DATE

SCALE 1:1

For Educational Use Only

MATERIAL

ALL DIMENSIONS IN mm

$0.7^{+0.1}_{0}$

25

20.5

$0.7^{+0.1}_{0}$

$\emptyset 11.35^{0}_{-0.1}$

$\emptyset 12^{0}_{-0.1}$

PIN_SMALL

PART NAME

DESCRIPTION:

QUANTITY:

PART #

DRAWN BY

MATERIAL

For Educational Use Only

ALL DIMENSIONS IN mm

$0.7^{+0.1}_{0}$

$0.7^{+0.1}_{0}$

31

26.5

$0.7^{+0.1}_{0}$

$\varnothing 11.35^{0}_{-0.1}$

$\varnothing 12^{0}_{-0.01}$

PART NAME
PIN

DESCRIPTION

DRAWN BY

SCALE
2:1

MATERIAL

ALL DIMENSIONS IN mm

QUANTITY

PART №

For Educational Use Only

$0.7^{+0.1}_{0}$

31

26.5

$0.7^{+0.1}_{0}$

$\emptyset 11.35^{0}_{-0.1}$

$\emptyset 12^{0}_{-0.01}$

PIN

PART NAME

DESCRIPTION

DRAWN BY

QUANTITY

PART N

MATERIAL

SCALE 2 : 1

For Educational Use Only

ALL DIMENSIONS IN mm

CGT

For Educational Use Only

$16^{+0.2}_{+0.1}$

$\varnothing 12$ ream

70

35

25

R5

2

5

13

Tap 5/8-18

26

26

26

FORK

PART NAME

DESCRIPTION

QUANTITY

PART #

DRAWN BY

MATERIAL

ALL DIMENSION IN mm

1:1

For Educational Use Only

For Educational Use Only

$8_{-0.1}^{0}$

$R6_{+0.1}^{+0.2}$

$9°$

$14_{0}^{+0.1}$

$24_{0}^{+0.1}$

$2-45°$

$10_{+0.1}^{+0.2}$

19.5

$\varnothing 5/8"$

$27_{0}^{+0.1}$

56

$R13.5$

JOINT

PART NAME

DESCRIPTION

DRAWN BY

PART N

QUANTITY

1:1

MATERIAL

ALL DIMENSIONS IN mm